

THE MOST LUMINOUS FAR-INFRARED EXTRAGALACTIC SOURCES

M. HARWIT AND J. R. HOUCK

Center for Radiophysics and Space Research, Cornell University

B. T. SOIFER¹

California Institute of Technology

AND

G. G. C. PALUMBO²

NASA/Goddard Space Flight Center, Greenbelt, Maryland

Received 1986 May 29; accepted 1986 September 23

ABSTRACT

Extremely luminous far-infrared sources are difficult to explain as active sites of star formation, because their ratios of optical-to-infrared luminosities are extremely low. We show that brief intervals during which interacting galaxies collide can account for extremely high ($\geq 10^{11} L_{\odot}$) luminosities. The small fraction of the population that exhibits extreme luminosity also roughly equals the fraction of spiral galaxies expected to be observed undergoing collisions at any given time. We propose a number of potential tests that would distinguish our model from others.

Subject headings: galaxies: structure — infrared: sources

I. INTRODUCTION

The most luminous sources identified through the *Infrared Astronomical Satellite (IRAS)* survey exhibit luminosities approaching or even exceeding $10^{12} L_{\odot}$ (Soifer *et al.* 1984*a, b*; Aaronson and Olszewski 1984; Wright, Joseph, and Meikle 1984; Allen, Roche, and Norris 1985; Houck *et al.* 1985; Lawrence *et al.* 1986). These luminosities are two to three orders of magnitude higher than those of most spiral galaxies. Infrared galaxies with luminosities in the range 10^{10} – $10^{11} L_{\odot}$ had been known before (Rieke and Low 1972; Telesco and Harper 1980), among them the frequently studied sources M82, NGC 253, and NGC 1068. These less luminous sources may be explained by postulating unusually high rates of star formation (Harwit and Pacini 1975). In star-forming regions, massive young stars and supernovae which evolve from them can provide the bulk of the energy that would have to be first absorbed and then reradiated by nearby dust clouds.

While the thought that star-forming regions also provide an explanation for the extremely luminous far-infrared sources (ELFS) first appears attractive, closer scrutiny reveals difficulties with this model and suggests a more plausible alternative. If these extreme ($L \geq 10^{11} L_{\odot}$) sources were active sites of star formation—as the less luminous, ordinary spirals frequently appear to be—then we would expect an accompanying high optical luminosity as well. To be sure, self-absorption by dust in massive aggregates of star-forming regions could act to lower the optical luminosity; but if we imagine a roughly spherical aggregate of such regions, its infrared-to-optical luminosity ratio would be proportional to the two thirds power of the far-infrared (FIR) luminosity: The optical luminosity would be proportional to the surface area of the aggregate, while the FIR luminosity would be proportional to the volume. This scaling law assumes that all the star-forming

regions in the aggregate are roughly similar, that they are more or less uniformly spread throughout the volume, and that only those regions that lie near the surface of the aggregate emit optical radiation that can escape.

Since the most luminous FIR sources have FIR luminosities 1000 times higher than ordinary spirals, we might expect their infrared-to-optical luminosity ratios to be 10 times higher than those of the ordinary spirals. Instead, we find that these ratios range up to 100:1 and show no particular correlation to the total luminosity. This suggests that while bursts of star formation can explain a large fraction of luminous infrared galaxies, some other mechanism than star formation might play a dominant role in producing the extreme luminosities. One possible mechanism is collisional heating of gas in strongly interacting galaxies, and we examine this possibility in the remainder of this paper.

We start with the observation that a fair fraction of galaxies has been classified as interacting. The circumstance leading to those interactions is not entirely clear, since the currently accepted intergalactic distances and the presumed random velocities of galaxies ($\sim 100 \text{ km s}^{-1}$) would make close interaction appear unlikely. It may be that galaxies originally formed in loose aggregates within clusters, or that capture into distant orbits took place during early epochs when galaxies were closer to each other. More recent perturbations of these loosely bound systems could then produce the close interactions currently observed.

The idea that interacting galaxies might be powerful emitters of infrared emission is not entirely new. As part of a classical investigation of interacting galaxies (Joseph *et al.* 1984), Wright, Joseph, and Meikle (1984) first noted that NGC 6240, an interacting pair of galaxies, is one of the most luminous extragalactic sources identified in the *IRAS* survey. Joseph, Wright and Wade (1984) observed emission from vibrationally excited molecular hydrogen in Arp 220 and NGC 6240 and suggested that these sources represent massive regions of shock-induced star formation. In contrast, we will argue here

¹ Visitor at Cornell University when this work was begun.

² NRC/NAS Research Associate, on leave from Dipartimento di Astronomia, Università di Bologna, Italy.

that the observed extreme luminosity is more likely to be derived from kinetic energy dissipated in the collision itself; and while star formation may well be triggered by the associated shocks, it is more likely that the star-forming stage follows at a somewhat later time, after much of the initial energy liberated in the collision of galaxies has dissipated and the extremely luminous FIR emission phase has subsided. This sequence of events seems to be more compatible with the observational evidence cited below.

In the next section we present data that have been accumulating on the ELFS. We then investigate the observational characteristics that high-velocity collisions between galaxies would exhibit. These expected traits are then compared to existing data, and a final section discusses the strength of the case that can be made for associating ELFS with colliding galaxies.

II. THE APPEARANCE OF ELFS

1. Luminosities of ELFS range up to $3 \times 10^{12} L_{\odot}$, for an assumed Hubble constant of $75 \text{ km s}^{-1} \text{ Mpc}^{-1}$. For the sample of six studied by Houck *et al.* (1985), none of the optical identifications appeared to have dominant active nuclei, though several investigators find that the $10 \mu\text{m}$ flux from ELFS is almost always associated with the centers of the optical images.

2. The FIR flux appears uncorrelated with the visual and near-infrared flux, which tends to hover within a factor of 3 from a value of $10^{10} L_{\odot}$ (Houck *et al.* 1985; Allen, Roche, and Norris 1985). The optical flux, therefore, is quite consistent with that of fairly normal spiral galaxies. Aaronson and Olszewski (1984) note that the $R-I$ colors of their sample of four identified sources is completely normal for disk galaxies. Similarly, Houck *et al.* (1985) also note that the $g-r$ colors are quite similar to those of normal galaxies, being consistent with, or perhaps up to 0.2 mag bluer than, those of giant elliptical galaxies at comparable redshifts. They find that these galaxies appear to have a "near normal stellar population, plus a powerful infrared source," a trait also noted by Aaronson and Olszewski.

3. Among all spirals, a proportion of 10^{-3} have luminosities as high as $10^{11} L_{\odot}$, and 2×10^{-6} have luminosities greater than $10^{12} L_{\odot}$ (Soifer *et al.* 1986). Lawrence *et al.* (1986) note a break in the luminosity function at $L \sim 10^{11} L_{\odot}$, suggesting that luminosities of $10^{11} L_{\odot}$ or higher may be the traits of a distinct class of sources.

4. Bright FIR galaxies ($L \geq 10^{10} L_{\odot}$) also tend to be among the brightest radio spirals with strong extended nuclear sources. The FIR flux is found to be directly proportional to the 21 cm continuum flux, provided the contribution of point-like sources is subtracted from the total 21 cm flux observed. (Helou, Soifer, and Rowan-Robinson 1985; Sanders and Mirabel 1985).

5. The FIR flux is generally correlated with the 2.6 mm CO flux, for the 23 FIR-emitting galaxies observed by Sanders and Mirabel (1985). Nondetections in CO and weak detections were largely confined to galaxies that had compact radio cores and emitted most of their radio continuum from a region smaller than 100 pc. The FIR luminosity is approximately proportional to the $3/2$ power of the 2.6 mm CO luminosity, as expected from an aggregate of optically thick CO clouds. Inferred H_2 masses are $\sim 2 \times 10^{10} M_{\odot}$ for the most luminous sources.

6. Houck *et al.* (1985) note that seven of eight ELFS identi-

fied showed peculiar galaxies or else a galaxy that was a member of a small group. Noting this general trend for extremely bright infrared galaxies, Soifer *et al.* (1984b) had already pointed out that galaxy interaction appears to be associated with these IRAS sources. Allen, Roche, and Norris (1985) noted that many ELFS appeared to be interacting, irregular, or disturbed. Sanders and Mirabel (1985), who were interested in radio-bright spirals, found that 80% of the galaxies in their sample of 25 showed evidence of interaction with a companion and that nearly three-quarters of the galaxies were subclassified as peculiar. Among the most luminous galaxies studied by Soifer *et al.* (1986), more than 70% of those having FIR luminosity greater than $5 \times 10^{11} L_{\odot}$ were interacting.

7. Many ELFS exhibit broad emission lines. Sanders and Mirabel (1985) observed the broadest CO emission lines for NGC 660, NGC 520, IC 4553 (= Arp 220), NGC 2623, and NGC 6240, galaxies which they "suspect of being strongly interacting contact pairs." Line widths range up to well over 500 km s^{-1} for Arp 220, the most luminous of the ELFS in their sample, at $10^{12} L_{\odot}$, where a Hubble constant of $75 \text{ km s}^{-1} \text{ Mpc}^{-1}$ has been assumed. Arp 220, NGC 6240, and NGC 2623 are among the four most luminous galaxies they observed, having line widths of $400\text{--}600 \text{ km s}^{-1}$. Only NGC 3690, with a luminosity somewhere between that of NGC 2623 and NGC 6240, exhibits CO emission lines less than 200 km s^{-1} wide. None of these measurements take projection effects into account. Broadened lines also were observed in many of the most luminous sources observed by Allen, Roche, and Norris (1985) in $\text{H}\alpha$ and $[\text{N II}]$. Their spectra were taken at low resolution, but the blend of the two lines could not be resolved in approximately a third of their sources, suggesting that at least one of the two lines was broadened with an upper limit of 1000 km s^{-1} full width at half-maximum. Aaronson and Olszewski's (1984) $\text{H}\alpha$ measurements on one of the most luminous sources, 0422+009, shows a line width corresponding to $\sim 600 \text{ km s}^{-1}$, and the $[\text{O II}] \lambda 3727$ line is similarly broadened.

8. Beck, Turner, and Ho (1986) and DePoy, Becklin, and Wynn-Williams (1986) also note unusually weak $\text{Br}\alpha$ and $\text{Br}\gamma$ emission in the ELFS, based on the line strength one would normally expect for a given FIR flux in starburst galaxies. DePoy *et al.* also use their observed low $\text{Pa}\alpha$ line strengths to derive a $\text{Ly}\alpha$ photon flux which is one or two orders of magnitude lower than would be normal for H II regions producing a comparable FIR flux. They note that starburst galaxies have an order of magnitude more $\text{Ly}\alpha$ emission per infrared photon than ELFS.

9. Allen, Roche, and Norris (1985) find that the $[\text{O II}] \lambda 3727/[\text{O III}] \lambda 5007$ line ratio is high for ELFS, with a value several times higher than for low-luminosity starburst galaxies for which French (1980) had found a ratio around 0.2. ELFS tend to have line ratios of 1.0 or higher for this line pair—on the order of or higher than the ratio found for the most luminous galaxies in the sample studied by French. Similarly, the $\text{H}\alpha/[\text{O III}]$ ratio also appears high when contrasted to French's sample. The $[\text{O III}]$ lines simply are very weak and sometimes undetected in the observations conducted by Allen *et al.* In studying the source 0422+009, Aaronson and Olszewski (1984) also found a notable absence both of $\text{H}\beta$ and of the $[\text{O III}]$ line. While the weak $\text{H}\beta$ flux could be attributed to extinction, the high $[\text{O II}]/[\text{O III}]$ ratio implies a low excitation temperature.

10. The X-ray emission from ELFS can be considerably

higher than the emission expected from massive star-forming regions. The X-ray emission from the star-forming regions in our Galaxy, as well as from such galaxies as M83 and M51, is quite low (Trinchieri, Fabbiano, and Palumbo 1985; Palumbo *et al.* 1985) when compared to the FIR flux: $L_X/L_{\text{IR}} = 5 \times 10^{-5}$. For M82 this ratio is rather higher, $\sim 3 \times 10^{-4}$ (Watson, Stanger, and Griffiths 1984); but ELFS can be significantly more powerful emitters of X-rays, though this is not universally the case. For NGC 520 that ratio is 1.5×10^{-3} (see Fabbiano and Trinchieri 1985). For NGC 4038 (Fabbiano, Feigelson, and Zamorani 1982), the corresponding ratio is also close to 10^{-3} . To be sure, Seyfert galaxies and emission-line galaxies can also have high X-ray emission rates; but standard regions of star formation do not appear to be powerful X-ray emitters.

III. THE PROBLEM

The problem to be faced is the construction of a model for ELFS which explains the dominant observed features:

1. A very high FIR luminosity associated with sources generally observed to be interacting galaxies having normal optical luminosities uncorrelated with the infrared luminosity but 21 cm radio continuum emission proportional to the FIR emission.

2. Low numbers of ionizing photons, given the high FIR luminosities.

3. Low ionization states of atoms optically observed in emission.

4. A FIR luminosity that increases as the 3/2 power of the CO luminosity.

5. Occasional powerful X-ray emission.

The model described in the next section appears to account satisfactorily for all these features. A starburst model of galaxies appears to fall short on at least the first three counts.

IV. THE MODEL

The model we employ to explain the observed characteristics of ELFS and to predict further observable features is based on a picture of colliding galaxies. We suppose that the galaxies have a central disk ~ 2 kpc in diameter containing giant molecular clouds, as well as more tenuous distributions of gas, as found in our own Galaxy and in many others. The molecular clouds are considered to have densities $n_{\text{H}} \approx 10^3 \text{ cm}^{-3}$ and to occupy regions that are only of order $Z \approx 90$ pc thick and thus to have masses of $\sim 6 \times 10^9 M_{\odot}$. Both n_{H} and Z are assumed to be relatively invariant as we go from one galaxy to the next, and the total mass of hydrogen involved is comparable to that inferred by Sanders and Mirabel (1985). We maintain that ELFS represent a direct collision of the central disks of two colliding galaxies. The more sparsely distributed clouds at larger distances from the centers of these galaxies are less likely to collide as the two galaxies pass through each other. (It may be worth noting here that Sanders, Solomon, and Scoville 1984 find a disk of the approximate dimensions we have assumed at the center of our Galaxy, but its total mass is much lower than our assumed density would imply.)

When the two galaxies collide, their relative approach velocity v_a typically will have a value of 500 km s^{-1} . That varies somewhat with distance from the galaxies' centers; but to the extent that rotation curves for galaxies are found to exhibit constant rotational velocities, $v_R \approx 250 \text{ km s}^{-1}$, over most of their disks (Rubin *et al.* 1985), we can figure on a spherical mass distribution with $M(r) \propto r$, where r is radial distance.

Infall into a galaxy having a mass $10^{11} M_{\odot}$ within 10 kpc of the center will then produce velocities in excess of 500 km s^{-1} in bodies penetrating to within 1 kpc of the center. We should therefore not be surprised to find that observed emission-line widths in the most luminous ELFS are of the order of 500 km s^{-1} , since these sources appear to be galaxies in collision.

Figure 1a shows the onset of collision. As the two galaxies collide, their respective molecular cloud layers will be preceded by tenuous halo gas and halo cosmic rays. The halo gas impinging on the leading surfaces of the molecular clouds will form thin ionized layers. It is not clear whether the halo cosmic rays will couple to these thin layers, or whether—as appears more likely from the account of Morfill, Meyer, and Lüst (1985)—they will pass right through the neutral clouds even before they have had time to form a sufficiently well developed ionized layer to couple to the cosmic rays. However, it is possible that some cosmic-ray acceleration does occur at this stage. We return to a discussion of cosmic-ray acceleration and radio emission in §§ XII and XIII.

As the molecular clouds interpenetrate—Figure 1b—gas from both molecular clouds becomes completely ionized. Each cloud develops a shock front with an intervening ionized layer. Initially this layer is sandwiched between the approaching molecular clouds. Ultraviolet radiation and energetic particles generated in the hot ionized layer can penetrate the molecular cloud, heating it and causing dust grains to radiate much of the impact energy in the FIR. This is the central claim of our model.

The ionized layer continues to get thicker (Figs. 1c and 1d) until all the molecular material has collided and become ionized (Fig. 1e). The density of the ionized layer at its surface is ~ 4 times that of the original molecular cloud density, since the shock is nearly adiabatic. Because the duration of the interpenetrating collision is ~ 1000 times longer than the cooling time for the ionized gas, the layer that emits ultraviolet radiation most intensely is thin and lies right behind the shock.

Once the two molecular layers have completely interpenetrated, the ionized gas begins to rapidly expand in a reverse shock that now couples strongly to the halo gas and cosmic rays previously in the lee of the molecular layers. The relative velocity of the expanding layer front and halo gases will be on the order of the initial approach velocity of the two galaxies at impact. At this stage halo cosmic-ray particles are efficiently accelerated, and their synchrotron radiation can give rise to the observed radio emission. If the two molecular layers are not equally thick, one layer will become completely ionized before the other. However, the remnants of the thicker layer will continue to stream into the ionized region, still at supersonic speeds, until both molecular layers have been completely consumed. Synchrotron radiation and cosmic-ray acceleration, however, may predominantly be produced through occasional collisions between more tenuous clouds in the disks of the two galaxies. Because of their lower densities, such colliding clouds radiate little of the impact energy away. Instead they become ionized and rebound almost elastically with expansion velocities of several hundred kilometers per second, acting much like nova or supernova shells (see § XIII).

V. ENERGY SUPPLY AND SOURCE STATISTICS

Consider two galaxies, each with a mass M_{H} in gas. Let all this gas collide during a time interval t , as the galaxies approach each other with a relative velocity v_a . If the galaxies

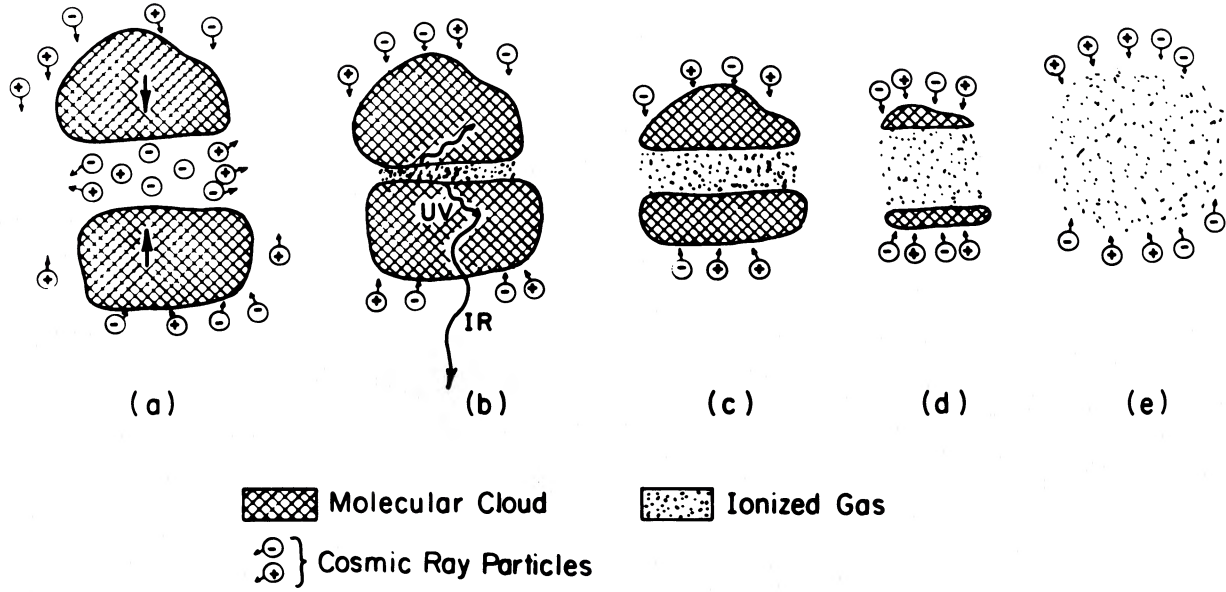


FIG. 1.—Schematic diagram of colliding gas clouds. Two molecular clouds approach. (a) Upon contact, the gas between them is ionized and heated to temperatures above 10^6 K. (b) Ionizing radiation escapes into the molecular gas and produces an ionized layer even before that gas has a chance to collide with the stationary layer of hot gas that has formed. (c)–(d) As the collision proceeds, the central layer thickens until no more molecular gas remains. (e) Then the hot outer layers of the ionized cloud expand outward to meet trailing, more tenuous halo gas from each of the colliding galaxies.

meet face on, and each gas layer has a thickness Z ,

$$t \approx 3Z/2v_a,$$

as we show in § VII. The final layer of mixed gas will have a velocity $v = v_a/2$ with respect to either galaxy, and the total kinetic energy deposited in this layer on collision is $M_H v_a^2/4$. If this energy is radiated away as rapidly as it is deposited in the ionized layer produced in the collision, the luminosity of the colliding gas clouds will be

$$\begin{aligned}
 L &\approx \frac{M_H v_a^3}{6Z} \\
 &\approx 1.5 \times 10^{45} \left(\frac{M_H}{2 \times 10^{43} \text{ g}} \right) \left(\frac{v_a}{5 \times 10^7 \text{ cm s}^{-1}} \right)^3 \\
 &\quad \times \left(\frac{2.7 \times 10^{20} \text{ cm}}{Z} \right) \text{ ergs s}^{-1}.
 \end{aligned}$$

That luminosity would persist for 8×10^{12} s, $\sim 3 \times 10^5$ yr, and would be using up $10^{10} M_\odot$ of gas in each galaxy. A mass of $10^{10} M_\odot$ corresponds to two central disks 2 kpc in diameter, 90 pc thick, with a density of atoms $n \approx 10^3 \text{ cm}^{-3}$. For galaxies that have total masses above $10^{11} M_\odot$ and gas content that could be of order $10^{10} M_\odot$, virtually all the mass of gas needs to collide to yield a luminosity of order $4 \times 10^{11} L_\odot$, for 3×10^5 yr. In a more oblique collision, the luminosity would be lower, but radiation could persist for up to $2R/v_a \approx 4 \times 10^6$ yr at $L \approx 4 \times 10^{10} L_\odot$. If every galaxy went through such a collision once during its existence of 10^{10} yr, we would find that roughly one galaxy in 2500 would be undergoing such a collision at any given time. This is somewhat lower than the fraction of all spirals, one in 10^3 , that Soifer *et al.* (1986) find to have $L \geq 10^{11} L_\odot$. It may also be compatible with the finding of Schweizer (1986), who thinks that $\sim 10\%$ of all galaxies have gone through a collision at some stage in their past.

VI. RELATIVE LUMINOSITIES PRODUCED IN COLLISIONAL DISSIPATION AND BY SUBSEQUENTLY FORMED STARS

We now compare the luminosities that one can expect from stars formed in the collision of two clouds, as compared to the luminosity produced in the dissipation of kinetic energy during the collision preceding star formation. To do this, some initial mass function must be assumed. Lequex (1985) compares a variety of initial mass functions, $\psi(m) = dn(m)/d \log m \approx A m^{-(2+x)}$, where m is the mass of the star and A is a constant. The Miller and Scalo (1979) function sets $x = 0$. The luminosities of these young main-sequence stars can be represented by $L = L_\odot (m/M_\odot)^{3+y}$, where y also is a small number. Then the luminosity-to-mass ratio for any aggregate of young stars can be written

$$\begin{aligned}
 \frac{L}{M} &= \frac{\int L dn(m)}{\int \psi(m) dm} \\
 &\approx \left(\frac{1+x}{1+y-x} \right) \frac{M_{\max}^{(1+y-x)} M_{\min}^{(1+x)}}{M_\odot^{(2+y)}} \left(\frac{L_\odot}{M_\odot} \right).
 \end{aligned}$$

For $x = y = 0$, a maximum stellar mass $M_{\max} \approx 60 M_\odot$, and a minimum mass $M_{\min} \approx 0.1 M_\odot$, one obtains $L/M \approx 6 L_\odot/M_\odot$. For extreme values, $y = 0.5$ and $x = -0.3$, $L/M \approx 125 L_\odot/M_\odot$. Denying the existence of stars with $M < M_\odot$ also can raise L/M by an order of magnitude. However, all this is to be compared to the luminosity produced in the dissipation of collisional energy, which for a total final mass $M = 2M_H$ can be obtained from our previous result:

$$\begin{aligned}
 \frac{L}{M} &\approx \frac{v_a^3}{12Z} \\
 &\approx 20 \left(\frac{v_a}{5 \times 10^7 \text{ cm s}^{-1}} \right)^3 \left(\frac{2.7 \times 10^{20} \text{ cm}}{Z} \right) \left(\frac{L_\odot}{M_\odot} \right).
 \end{aligned}$$

Hence, only the assumption of conversion of most of the colliding gas into stars—as contrasted to a contention that perhaps less than 10% of the gas is actually converted into stars—or else extreme luminosity functions or extreme initial mass functions would give newly formed stars a luminosity comparable to energy dissipated in a collision. Moreover, stars formed early during an oblique collision of galaxies would later appear denuded of their dust cocoon and would provide an amount of visible starlight far in excess of the observed. Nor is there sufficient time to form supernovae still surrounded by dust: star bursts simply do not appear capable of providing the high infrared and low optical luminosities of the cloud collisions that must precede them.

VII. IMPACT PROBABILITIES

Consider two thin, cylindrical slabs, A and B, beginning to collide. Figure 2 shows some of the relevant parameters that enter the interaction. An angle θ characterizes the tilt between the two slabs, which, for simplicity, are assumed to have equal radius R and thickness Z . The velocity of approach of one galaxy toward the other is v_a , a vector whose direction makes an angle ϕ with respect to the perpendicular drawn to slab B. Angles θ and ϕ lie in planes separated by an angle ψ . Slab A is chosen to be the one whose rim first touches slab B at some distance a from that disk's rim. The diagonals drawn through the touching-point cross at an angle α when projected on the plane of slab B. In viewing Figure 2, it is important to keep in mind that angles take on values only $0 \leq \theta \leq \pi/2$, $0 \leq \alpha < 2\pi$, and that v_a does not generally lie in the plane of the paper. The distance a is measured to the nearest rim on slab B toward which the vertex of angle θ approximately points. ψ is measured from the plane in which angle θ lies, and about an axis perpendicular to slab B. An angle $\psi = 0$ places the angles θ and ϕ in the same plane, in our case the plane of the page. Note that when $\psi = \pi$ and $\phi = \pi/2 - \theta$, slab A slices through slab B along its own plane. In that case, only a swath of thickness Z is cut out of slab B in the collision, and slab A suffers no more than some ablation at its leading edge. In such a collision, the total volume of the swath removed from slab B—galaxy B—amounts only to

$$V \approx Z^2 D / \sin \theta,$$

where D (see Fig. 2c) depends on α but is of order $D \approx R$. This volume V is small compared to that for a collision with $\psi = 0$, unless the angle θ is very small; then we have virtually a face-on collision, for which angle ψ becomes relatively unimportant. Estimation of the probabilities of different configurations leading to what might be identical luminosities L , produced under quite different combinations of the parameters a , θ , α , ϕ , ψ , is quite complex, mainly because each of these parameters varies independently. Nevertheless, it is important to try to obtain a rough estimate of the probability distribution $P(L/L_{\max})$ to compare to the actual distribution of luminosities observed. Here L_{\max} is taken to be that luminosity produced when $\theta = \alpha = \phi = a = 0$, the face-on collision in which the angle ψ has no significance.

Note that in a realistic case, we would also have to consider slabs of different radii R , densities n , and thicknesses Z , having velocities v_a also distributed over a range of values. And if one wanted to be even more realistic, slabs of unequal sizes and densities would need to be taken into account. The profusion of parameters rapidly escalates.

In order to arrive at some reasonable approximation to the

probability distribution of luminosities, we neglect many of these possibilities and make the following simplifications.

1. We know that $Z \ll 2R$. For $Z = 90$ pc and $R = 1$ kpc, $Z/2R = 0.045$. We therefore lump all collisions together in which one galaxy slices through the other and assign them a luminosity around $L_{\max}/20$. Such collisions will include cases in which $|\theta|$ or ϕ has values in excess of $5\pi/12$, or 75° . It will also include cases in which $\psi = \pi$ and $\phi = \pi/2 - \theta$, as discussed above. These constitute about half of all the collisions taking place.

2. We consider the length X shown in Figure 2b to be that length measured on slab A which eventually can interact with slab B. It is a measure of the collisional overlap. When ψ has a value $\pi/2$ and ϕ is close to 75° , the motion of slab A with respect to slab B is downward in Figure 2b but also out of the plane of the page, and the concept of a length X is somewhat ill defined. For present purposes, however, we will assume that we can average over all angles ψ and ϕ , and that the length X on slab A interacting with slab B is $X(\alpha, \phi)$. When the angle ϕ is not too large—i.e., $\phi \leq 75^\circ$ —then $X(\alpha, \phi)$ is not too sensitive to ϕ , and we will approximate $X(\alpha, \phi)$ by $X(\alpha)$ chosen for two extreme angles $\alpha = 0$ or $\pi/2$, for which, respectively, $X(\alpha) = (2R - a)$ or $[(2R - a)a]^{1/2}$. These are extremes, since the case $0 < \alpha \leq \pi/2$, $a \leq R$ is the same as $\pi/2 \leq \alpha < \pi$, $a \geq R$.

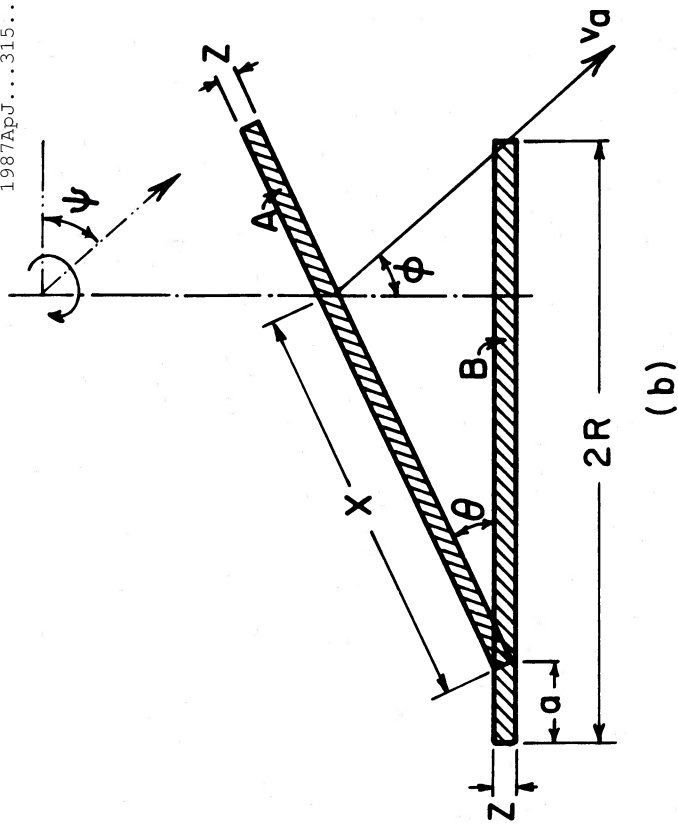
We are now close to establishing a probability function for the different interaction parameters a , θ , α , ϕ to be observed. However, we first note that the probability of *observing* a given set of interaction parameters in an ongoing collision differs from the actual probability of occurrence. To see that, we need only note that a face-on collision, $\theta = \phi = 0$, takes place in a time of order $3Z/2v_a$, while a collision at larger angles θ , ϕ has a duration

$$t = \frac{X(\alpha) \sin \theta}{v_a \cos \phi}, \quad \theta \geq \frac{2Z}{\pi R}.$$

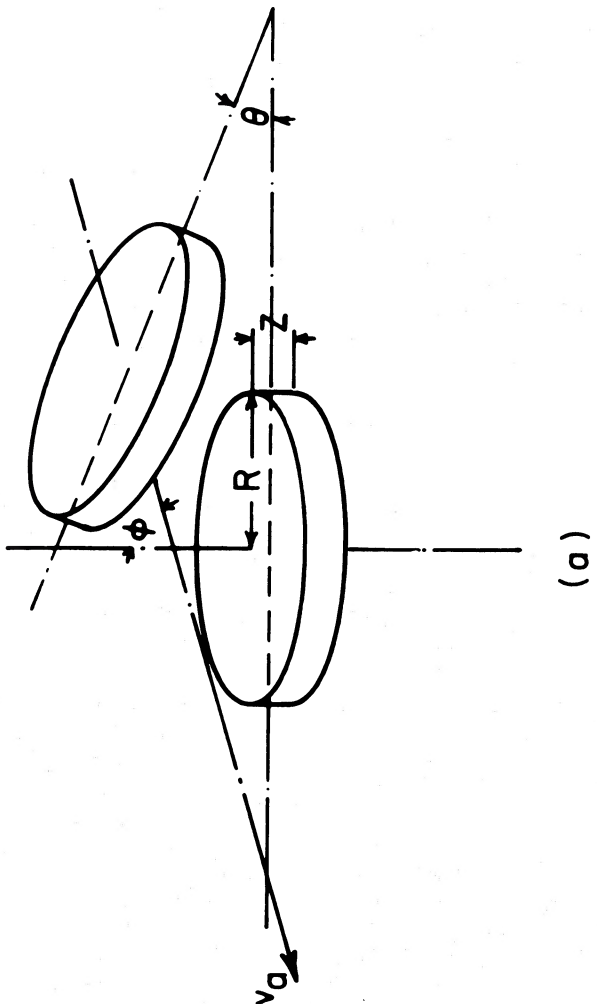
We therefore have to take the probabilities for occurrence, $P(\alpha) = 1/(2\pi)$, $P(\theta) = \sin \theta$, and $P(\phi) = \sin \phi$, as well as the interaction time t , into account in setting up a probability for observing interactions at these angles. Finally, also, we need a probability for the occurrence of parameter a . This is just $P[a] = 2[R - a]R^{-2}$. With these considerations in mind we can now set up a probability function for the range of angles $2Z/\pi R < \theta < 75^\circ$, $0 < \phi < 75^\circ$, where the lower bound on θ simply represents those angles sufficiently small to keep slabs A and B in contact along their entire overlapping faces throughout most of the collision:

A. For small angles $\theta \leq 2Z/\pi R$, the probability $P(\theta)$ of being in this angular range is $P(\theta) = 2Z^2/\pi^2 R^2$. The probability for any particular angle α is $(1/2\pi)d\alpha$, $P(\alpha) = 1/(2\pi)$. The probability of approach at any angle ϕ is $\sin \phi d\phi$, but the projected cross section—relative probability for collision with slab B—is proportional to $\cos \phi$. Hence $P(\phi) = \sin \phi \cos \phi$. The time of transit is $t = 3Z/2v_a \cos \phi$. Also, $P(a) = 2|R - a|/R^2$. Hence we have a probability proportional to

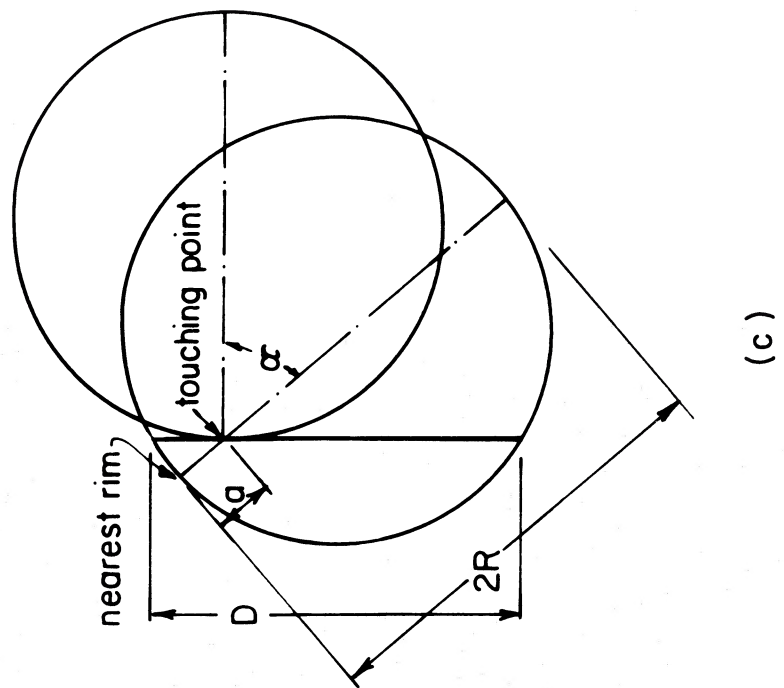
$$\int_0^{2Z/\pi R} P(a, \theta, \alpha, \phi) d\theta \propto \frac{3Z}{2v_a \cos \phi} \frac{1}{2\pi} \frac{2Z^2}{\pi^2 R^2} \\ \times \sin \phi \cos \phi \frac{2|R - a|}{R^2} = \frac{3Z^3 |R - a| \sin \phi}{\pi^3 R^4},$$



(b)



(a)



(c)

FIG. 2.—Explanation of the parameters that describe the configuration of colliding disks of gas. (a) Perspective drawing, (b) side view, (c) top view.

for $\theta \leq 2Z/\pi R$, $\phi \leq 75^\circ$. The luminosity under these conditions is

$$L \approx L_{\max} \frac{X(\alpha)}{2R} \cos \phi,$$

with $X(\alpha)$ equal to either $(2R - a)$ or $[(2R - a)a]^{1/2}$, each value having equal probability.

B. For larger angles, $P(\theta) = \sin \theta$. As discussed above, we also have $P(\phi) = \sin \phi \cos \phi$, $P(\alpha) = 1/(2\pi)$, $P(a) = 2|R - a|/R^2$, but $t = X(\alpha) \sin \theta/v_a \cos \phi$. Hence the probability distribution is proportional to

$$\begin{aligned} P(a, \theta, \alpha, \phi) &\propto \frac{X(\alpha) \sin \theta}{v_a \cos \phi} \frac{1}{2\pi} \sin \theta \frac{2|R - a|}{R^2} \sin \phi \cos \phi \\ &= \frac{X(\alpha) \sin^2 \theta |R - a|}{\pi v_a R^2} \sin \phi, \\ L &\approx \frac{L_{\max}(3Z/2) \cos \phi}{X(\alpha) \sin \theta} \frac{X(a)}{2R} \\ &= L_{\max} \left(\frac{3Z}{4R} \right) \frac{\cos \phi}{\sin \theta}, \end{aligned}$$

for $\theta \leq 2Z/\pi R$, $\phi \leq 75^\circ$. But since L is thus independent of $X(\alpha)$ and of a , we need consider only the angular dependence

$$P(\theta, \phi) = (4/\pi) \sin^2 \theta \sin \phi,$$

for $2Z/\pi R \leq \theta \leq 75^\circ$, $\phi \leq 75^\circ$. Here the factor $4/\pi$ normalizes the probability distribution. Integration up to $\theta, \phi = 75^\circ$ also shows that half the collisions involve angles $\theta, \phi \leq 75^\circ$ and half $\theta, \phi \geq 75^\circ$, as already mentioned above. We therefore consider three cases:

$$\text{Case 1: } P = \frac{1}{2},$$

$$L = L_{\max}/20,$$

where ϕ and/or $\theta \geq 75^\circ$

$$\text{Case 2: } P(\theta, \phi) = \frac{4}{\pi} \sin^2 \theta \sin \phi,$$

$$L(\theta, \phi) = L_{\max} \frac{2Z \cos \phi}{\pi R \cos \theta},$$

where

$$\frac{2Z}{\pi R} \leq \theta \leq 75^\circ, \quad \phi \leq 75^\circ, \quad Z \ll R.$$

$$\text{Case 3: } P(a, \phi) \approx \frac{2Z^2 |R - a| (\sin \phi)}{\pi^2 R^4},$$

$$L \approx \frac{L_{\max} X(\alpha) \cos \phi}{2R},$$

where $\theta \leq \frac{2Z}{\pi R}$, $\phi \leq 75^\circ$, $0 \leq \alpha \leq 2R$, $Z \ll R$,

$$X(\alpha) = \text{either } (2R - a) \text{ or } \sqrt{(2R - a)a},$$

each with probability $P(a, \phi)/2$.

Here all the probabilities are normalized; the integrated probabilities for cases 1 and 2 are 0.50 each; the integrated probability for all angles ϕ and parameters a for case 3 is $\sim 1.2 \times 10^{-3}$. The coefficient for the luminosity in case 2 has been chosen to make the case 2 and case 3 luminosities identical at $\theta = 2Z/\pi R$ and $X(\alpha) = 2R$.

Although the angle $2Z/\pi R$, in our case, is $3^\circ 28'$, we take the typical luminosity for this range of angles L_{\max} to be the value of L obtained at a slightly smaller angle: $2^\circ 86'$. We note, right away, that the θ -dependence is critical in determining the luminosity distribution, since the luminosity is particularly high for small angles θ , which have the lowest probability. Figure 3 shows the luminosity distribution derived on this simplified basis. It is fitted to the luminosity distribution of the most luminous *IRAS* galaxies reported by Soifer *et al.* (1986). The curve drawn through the points was computed with the aid of a rough numerical scheme in which the tilt angle of interaction θ was considered first. This is the most sensitive parameter determining the luminosity. Then the effects of increasing angles ϕ and off-axis collision parameter a were successively computed to determine the shape of the curve. The curve then was anchored to one specific point, roughly in the scatter of high-luminosity observations around $L = 10^{12} L_\odot$. That provides the sole arbitrary parameter, once the disk thickness-to-diameter ratio $Z/2R$ has been fixed at $90 \text{ pc}/2000 \text{ pc} = 0.045$. The shaded area at low luminosities and above the bold curve represents a somewhat arbitrary distribution of low-luminosity galaxies added on, to double the total number at $L/L_{\max} < 1/20$, to take into account all the galaxies that slice through each other, as already discussed.

In this connection it is interesting that Lawrence *et al.* (1986), who have investigated the distribution of luminosities in galaxies down to substantially lower luminosities where more normal galaxies also contribute, have found a break in their curve just below $3 \times 10^{10} L_\odot$, approximately where we also show a flattening.

It remains to establish that the absolute collision frequency implied by our model also makes sense. We note first that the probabilities we have shown are all normalized to one and the same observing time, which is the longest duration we would expect for a collision. That time is roughly $2R/v_a = 4 \times 10^6 \text{ yr}$. Soifer *et al.* (1986) estimate that one galaxy in 5×10^5 has a luminosity above $10^{12} L_\odot$. The computations leading to Figure 3 showed that one in 5000 galaxies with colliding central disks will have this peak luminosity. Roughly one galaxy in every 100 would therefore have to be in collision at the present epoch, to give the observed number of ELFS. This fraction is not vastly different from the fraction of galaxies observed to be peculiar. However, put differently, typical galaxies would have to collide once in $4 \times 10^8 \text{ yr}$, on the average, in order to produce the observed number of high-luminosity collisions. That rate might appear high. But two circumstances should be noted. Figure 3 involves an arbitrary choice of a point at which the theoretical curve is anchored to the data. If we had chosen $v_a \approx 600 \text{ km s}^{-1}$ and $M_H \approx 2 \times 10^{10} M_\odot$, we would have been justified in sliding the theoretical curve downward a factor of 10 and to the right a factor of 2. In that case, the break point at $10^{11} L_\odot$ would only be slightly shifted to $\sim 2 \times 10^{11} L_\odot$, and the number of required collisions would decrease by an order of magnitude. We also note that if galaxies formed loosely bound aggregates at some early epoch, relatively frequent collisions could be expected. Many of the

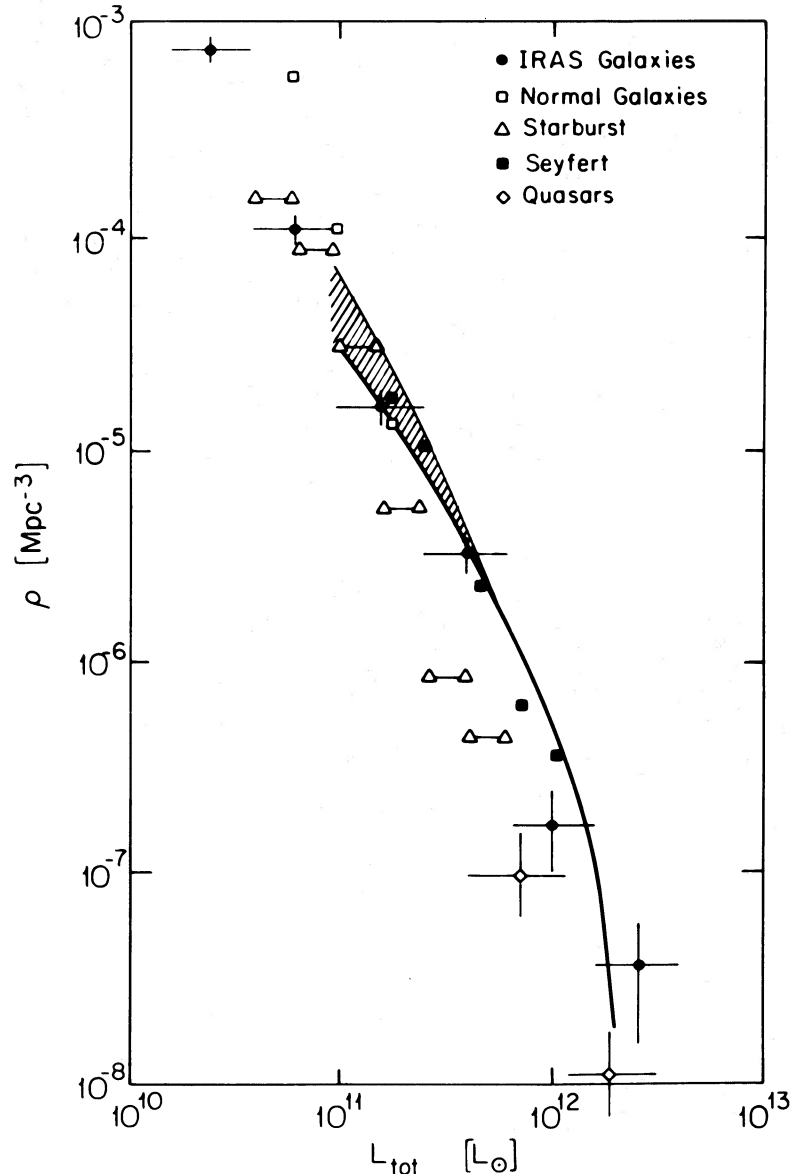


FIG. 3.—Luminosity distribution of the most luminous *IRAS* galaxies reported by Soifer *et al.* (1986). The curve drawn through the points is discussed in the text. It was computed in a rough numerical scheme in which the tilt angle θ of interaction was considered first. This is the most sensitive parameter determining the luminosity. Then the effects of increasing angles ϕ and off-axis collision parameter a were successively computed to determine the shape of the curve. The curve then was anchored to one specific point, roughly in the scatter of high-luminosity observations around $L = 10^{12} L_{\odot}$. That provides the sole arbitrary parameter, once the disk thickness-to-diameter ratio $Z/2R$ has been fixed.

collisions would occur quite ineffectually, most of the gas in the galaxies remaining unconsumed by the collision. However, there would be a fairly large number of successive collisions, some of which would be well centered.

In summary, rough calculations of the luminosity distribution of colliding galaxies suggest that the model we have in mind produces a reasonable fit. The absolute number of collisions required by our model calls for a higher collision frequency than most authors have been willing to admit. But the case can be made that these higher collision rates are reasonably consonant with observations.

VIII. RAPIDLY COOLING SHOCK SANDWICH

When two molecular clouds collide, a sandwich (Fig. 4) of ionized gas is created between them if the approach velocity v_a is sufficiently high. Each side of the sandwich is effectively being approached by gas at velocity $v = v_a/2$ for clouds of equal density (the assumption made here). At high collisional speeds v , where the fraction of the incident energy going into ionization or dissociation is negligible, an adiabatic shock effectively arises on each face of the layer. Most of the translational energy goes into heating the ionized gas.

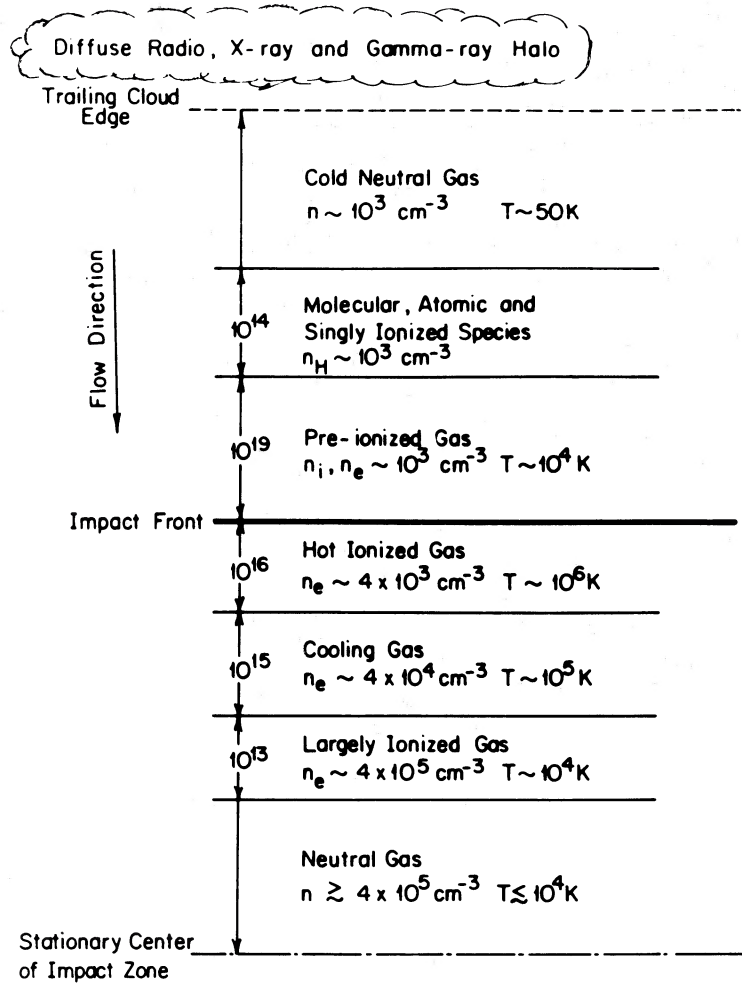


FIG. 4.—Layered structure of colliding clouds. At the bottom is the central portion of the colliding disks, at the top the outer precollision gas.

If we set the compression ratio—the ratio of densities ρ_o on the outgoing to ρ_i on the incoming side of the shocks—equal to

$$\Psi \equiv \frac{\rho_o}{\rho_i} = 4$$

for an adiabatic shock (e.g., Harwit 1973), electron and proton densities individually will be 4 times as high as the incident atomic hydrogen density. Continuity requires that the velocities v_o, v_i obey the relations

$$\rho_o v_o = \rho_i v_i, \quad v_o = v_i/4,$$

and

$$v = v_i - v_o = 3v_i/4.$$

From this, incidentally, we also see that the time t required to complete impact is

$$t = Z/v_i = 3Z/2v_a.$$

Pressure equilibrium demands

$$P_o + \rho_o v_o^2 = P_i + \rho_i v_i^2,$$

so that

$$\begin{aligned} P_o &= P_i + \rho_i v_i \left(\frac{3v_i}{4} \right) \\ &= P + \frac{4}{3} \rho v^2, \end{aligned}$$

where we have changed notation and set pressure $P \equiv P_i$ and density $\rho \equiv \rho_i$. Since $P \ll P_o$, $P_o \approx 4nmv^2/3 \approx 2n_e kT \approx 8nkT$, where T is the temperature, n_e is the electron density in the ionized gas, and $n_e = 4n$. We obtain

$$T \approx \frac{mv^2}{6k} \approx 1.2 \times 10^6 \text{ K} \left(\frac{v}{2.5 \times 10^7} \right)^2 \left(\frac{m}{1.6 \times 10^{-24}} \right),$$

in reasonable agreement with a far more comprehensive treatment by Hollenbach and McKee (1979).

At this temperature the cooling rate is $\mathcal{L} = 10^{-22}$ ergs $\text{cm}^3 \text{s}^{-1}$; and the rate at which a layer of thickness d radiates, in steady state conditions, is

$$n_e^2 \mathcal{L} d = 16 \times 10^{-22} n^2 d = \left(\frac{nmv^3}{2} \right).$$

Here, the last term on the right is the supply rate for mechani-

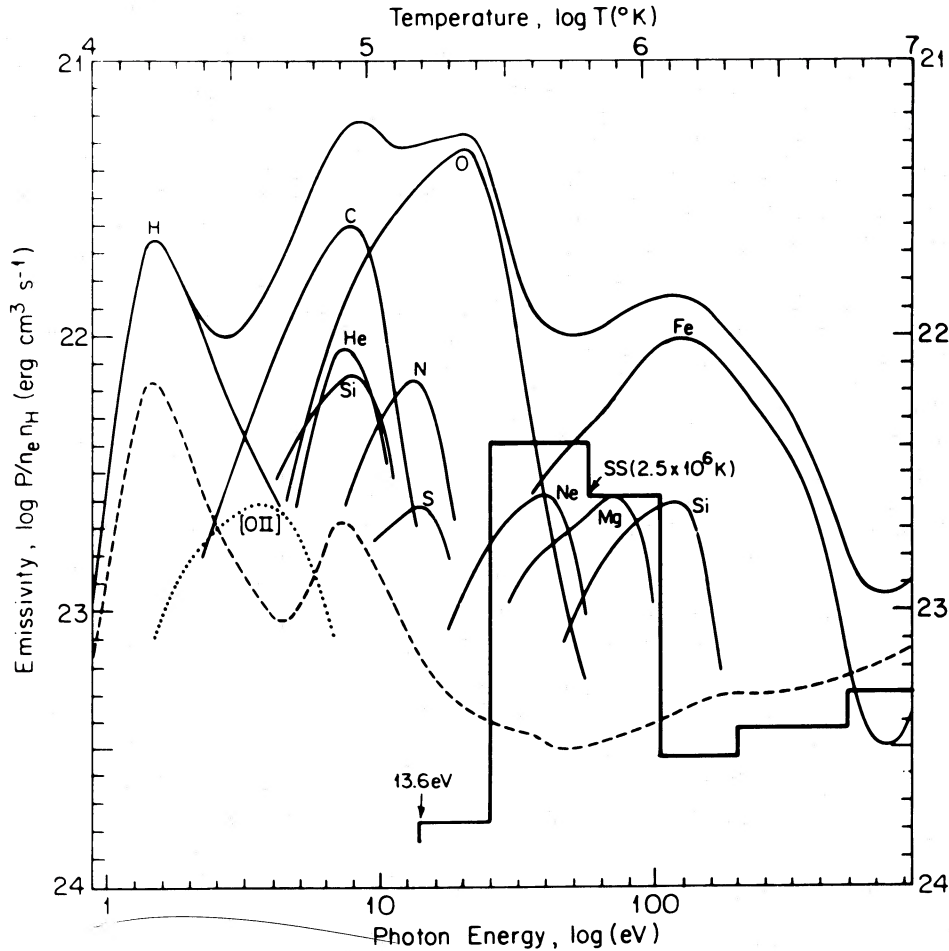


FIG. 5.—Cooling of hot ionized gases, after Gaetz and Salpeter (1983). The temperature scale at the top refers to the total emissivity shown by the topmost curve and the emissivity due to individual atomic and ionized species shown by the continuous curves labeled according to the contributing species. Normal abundances are assumed. The segmented curve labeled “SS(2.5×10^6 K)” is the summed spectrum computed for a temperature of 2.5×10^6 K. The energy scale at the bottom refers to the energy distribution of this emission. The emissivity shown for the highest energy bin drawn here actually is the mean emissivity for the energy range from 500 to 3000 eV, a range which would have extended beyond the right-hand edge of the plot if drawn to scale.

cal energy incident on the ionized layer from its two faces. Equilibrium between energy supplied and energy radiated away is reached only when the layer attains a thickness

$$d = 7.8 \times 10^{15} \left(\frac{m}{1.6 \times 10^{-24} \text{ g}} \right) \left(\frac{v}{2.5 \times 10^7 \text{ cm s}^{-1}} \right)^3 \times \left(\frac{10^3 \text{ cm}^{-3}}{n} \right) \left(\frac{10^{-22} \text{ ergs s}^{-1} \text{ cm}^3}{\mathcal{L}} \right) \text{ cm}.$$

Cooling of the ionized layer takes place primarily through allowed radiative transitions, Figure 5 (cf. Gaetz and Salpeter 1983). Radiation leaving the layer is readily absorbed far-ultraviolet emission which partially ionizes the molecular layer, partly contributes to excitation of atomic or molecular states, and largely ends up in grains which reradiate the absorbed energy at FIR wavelengths.

The heat content of the ionized gas is $3n_e kT$ per unit volume. At the temperature of 1.2×10^6 K calculated above, that amounts to 2.0×10^6 ergs cm^{-3} . The cooling time at the

cooling rate previously calculated will be

$$\tau = \frac{3n_e kT}{n_e^2 \mathcal{L}} = 1.24 \times 10^9 \left(\frac{10^{-22} \text{ ergs s}^{-1} \text{ cm}^3}{\mathcal{L}} \right) \times \left(\frac{4 \times 10^3 \text{ cm}^{-3}}{n_e} \right) \left(\frac{T}{1.2 \times 10^6 \text{ K}} \right) \text{ s}.$$

This is rapid compared to the interpenetration time, so that a steady state becomes established. Thomson scattering, with a cross section σ_e , is the main source of opacity at these high temperatures and low densities. The ionized gas therefore is largely transparent to the radiation it emits, since column densities nZ of order $\sigma_e^{-1} \approx 10^{24} \text{ cm}^2$ never appear to be approached in the molecular cloud layers or in the ionized layer to which they give rise.

It is worth noting that the cooling function \mathcal{L} has a maximum, at temperatures between 7×10^4 and 5×10^5 K, where its value is $\sim 10^{-21}$ ergs $\text{s}^{-1} \text{ cm}^3$, roughly 10 times higher than at 10^6 K (Gaetz and Salpeter 1983). At even lower tem-

peratures, \mathcal{L} drastically drops by two orders of magnitude until a temperature of 10^4 K is reached, where \mathcal{L} tends to level off at $\sim 10^{-23}$ ergs s^{-1} cm^3 . As the temperature drops, the density increases and the cooling rate is always higher than it was at 10^6 K. When temperatures around 10^4 K in the post-shock region are reached, magnetic pressures will become significant and will hinder further density increase or collapse if the initial molecular cloud fields are as high as $B \approx 5 \times 10^{-5}$ gauss.

One further comment concerns the emission of FIR fine-structure lines reminiscent of those observed by Shure *et al.* (1983) in planetary nebulae. The layers at 10^6 K should be detectable in their [Ne v] 24.28 μm and [O iv] 25.87 μm lines, features one would not expect from starburst galaxies where gas temperatures are far lower.

At 1.4 GHz, $T \approx 10^6$ K, $n_e \approx 4 \times 10^3$ cm^3 , the free-free opacity is $K \approx 1.4 \times 10^{-21}$ cm^{-1} . A layer of thickness $d = 7.8 \times 10^{15}$ cm, therefore, has emissivity $\sim 10^{-5}$. At frequencies below 5 GHz it emits less than 10^{-5} of its total radiated energy. Since $K \propto n^2 T^{3/2}$ and the radiated energy is proportional to KT , the free-free surface brightness of this layer actually is less at 10^6 K than when the layer cools to lower temperatures where densities, additionally, also are higher. Around 10^4 K, the total free-free emission radiated will be proportional to the Ly α flux roughly in the same way as for an H II region. But for ELFS, this is a low fraction of the FIR flux. This comes about because most of the ultraviolet emission at 10^6 K is converted into FIR radiation, implying that most of the 100 eV given up per atom on collision with the stationary layer goes into the FIR, and only one Ly α photon then results per extreme UV photon.

IX. SURVIVAL OF DUST GRAINS IN IONIZED PRESHOCK GASES

One might think that the dust in the colliding molecular clouds would quickly be destroyed through sputtering, when ionizing radiation enters the preshock regions and ionizes the gas there. That this is not so, however, hinges on the relatively low photon flux F actually leaving the shocked region. If that flux is beneath a critical value discussed within this section, below, the gas will remain cool and sputtering will be a minor effect. The flux is

$$F = \frac{nmv^3}{2} = 12.5 \left(\frac{n}{10^3 \text{ cm}^{-3}} \right) \left(\frac{m}{1.6 \times 10^{-24} \text{ g}} \right) \times \left(\frac{v}{2.5 \times 10^7 \text{ cm s}^{-1}} \right)^3 \text{ ergs cm}^{-2} \text{ s}^{-1},$$

which, we note, is low in comparison to the flux crossing the ionization front in some Galactic H II regions.

The efficiency with which the escaping photons ionize the neutral cloud depends in part on the energy distribution among photons (Fig. 5). The ionizing photon flux leaving the shock will be

$$F_i \approx 4 \times 10^{11} \left(\frac{20 \text{ eV}}{hv} \right) \text{ photons cm}^{-2},$$

where hv is a typical photon energy.

We now consider two energy groups of photons separately. Those with energies well above 2 rydbergs penetrate an order of magnitude deeper into the cloud than lower energy photons and release a smaller overall fraction of their energy in heat. Because higher energy photons penetrate further into the cloud

before ionizing an atom, their heating effect is distributed along a longer column of gas, and this factor more or less compensates for the higher amounts of heating such photons contribute. Since it is hot ionized gas that sputters grains most effectively, these higher energy photons will not significantly affect sputtering rates.

We can therefore consider the sputtering to be most severe if we look at the heat deposited closer to the ionization front by photons with energy between 1 and 2 rydbergs. One finds that almost independent of the spectrum of radiation, the flux F provides a heating rate per cubic centimeter of

$$R = 10^{-14} \left(\frac{F}{12.5 \text{ ergs cm}^{-2} \text{ s}^{-1}} \right) \times \left(\frac{n}{10^3 \text{ cm}^{-3}} \right) (1 - X) \text{ ergs cm}^{-3} \text{ s}^{-1}.$$

Here X is the fractional ionization state of the preshock gas. Even if as much as 10 eV per ionization goes into heating the gas, the gas temperature will only reach 6×10^4 K, and the heat content will be

$$10^{-8} \left(\frac{n}{10^3 \text{ cm}^{-3}} \right) \text{ ergs cm}^{-3}$$

for the densities assumed. At this temperature and density the cooling rate is 10^{-16} ergs cm^{-3} s^{-1} (Fig. 5), and one requires $\sim 10^8$ s for the gas to cool to $\sim 1.5 \times 10^4$ K. Draine and Salpeter (1979), however, have shown that silicon, iron, and graphite cores are negligibly sputtered at these temperatures, during the time the cloud cools itself—roughly 3 yr. And, depending on the model assumed for the ice, the layer sputtered off at 6×10^4 K will amount to only $3\text{--}30 \times 10^{-4} n$ \AA yr^{-1} . At our densities that would correspond to 10–100 \AA all told.

The grains therefore are not significantly sputtered, because gas cools itself rapidly after initial ionization—the cooling radiation ultimately escaping the cloud, usually through absorption and re-emission at FIR wavelengths by grains in the cloud.

There is only one way for sputtering to become serious. That would be for highly energetic photons to ionize the gas rapidly enough, so that the photoelectrons ejected from atoms had no time to give up their energy in ionizing still-neutral atoms. One could then end up with a fully ionized plasma in which electron temperatures were on the order of 10^6 K and where that energy only gradually was shared with protons. The plasma then would have a final temperature of several times 10^5 K. In our case, however, electrons need only a time

$$t_e \approx [(1 - X)n\sigma_e(3kT/m_e)^{1/2}]^{-1}$$

to lose energy through ionization, which for $\sigma_e \approx 8 \times 10^{-17}$ cm^2 and $T \approx 5 \times 10^5$ K is $t_e \approx 2.6 \times 10^4 (1 - X)^{-1}$ s. In contrast, the photoionization time for atoms with a cross section $\sigma_p \approx (v_0/v)^3 \times 10^{-17}$ cm^2 at frequencies v above the ionization edge v_0 , and at the above-cited photon flux is $t_p \approx (F_i \sigma_p)^{-1} \approx 2.5 \times 10^5 (v/v_0)^3$ s. For ionization fractions X below $\sim 95\%$, electrons, therefore, can lose their energy rapidly; and above that there are too few energetic electrons to make a significant temperature difference.

We may still calculate the grain temperature in the ionized preshock region. If the entire energy flux F is absorbed by grains of radius $a \approx 500$ \AA and emitted at wavelengths typically $\lambda_T \approx 50$ μm , grain radiation efficiency become $\lambda_T/a \approx 3$

$\times 10^4 T^{-1}$, and grain temperatures will be

$$T \approx [7.5 \times 10^3 (F/\sigma)]^{1/5} \\ \approx 70(F/12.5 \text{ ergs cm}^{-2} \text{ s}^{-1})^{1/5} \text{ K},$$

where σ is the Stefan-Boltzmann constant. These temperatures roughly correspond to the *IRAS* 60 $\mu\text{m}/100 \mu\text{m}$ color temperatures and are too low to lead to sublimation of grain ice mantles.

As a final consideration, we need to ask whether a shock front precedes the ionization front into the molecular cloud. With $F_i \approx 4 \times 10^{11}$ ionization photons $\text{cm}^{-2} \text{ s}^{-1}$ incident on the gas with atomic density $n \approx 10^3 \text{ cm}^{-3}$, the ionization front proceeds at a speed of $\sim 4 \times 10^8 \text{ cm s}^{-1}$. While the harder photons will always penetrate well beyond the front at which ionization is virtually complete, partially ionizing and partially heating the predominantly neutral cloud ahead of the ionization front, these photons cannot establish a shock of significant proportions. To be sure, the gas ahead of the ionization front will be heated, have its pressure increased through absorption of the hard photons, and seek to expand into the cooler gas, possibly even at supersonic speeds. Those speeds, however, are always going to be slow in comparison to that of the ionization front, since the gas temperature is so low. At any rate, dust absorption eventually begins to dominate, as discussed in § XI, and then the ionization front simply propagates at the speed $v_i = 4v/3$. Any shock that develops will therefore stay a constant distance in front of the ionization front, never able to outrun it. The gas crossing the ionization front will therefore not have been compressed to higher density and will have the same mass densities on both sides of the front.

X. ENERGY DEPOSITION IN THE MOLECULAR GAS

We just saw that a precollision layer of fully ionized gas develops even before the rapid heating, which takes place when the gas plows into the stationary sandwiched layer. There, the gas can only cool itself through ultraviolet emission, which escapes the hot ionized layer and typically penetrates deep into the ambient neutral region before producing secondary electrons through ionization.

Shull and Van Steenberg (1985) have examined the various ways in which energetic electrons give up their energy to ambient gas. The range of electron energies they investigated reaches up to several kilovolts and covers the regime of interest to us. They show that the fraction of a primary electron's energy deposited in the form of heat—as contrasted to ionization or excitation—is almost independent of electron energy at primary electron energies above $E_0 \approx 100 \text{ eV}$. It does, however, depend on the ionization fraction $n(\text{H}^+)/n(\text{H}_{\text{tot}})$ of the ambient gas: in a fully ionized gas all of the electron's energy losses go into heating. In a predominantly neutral cloud only 1/10 the electron's energy loss goes into heat, while the remainder is distributed almost equally between ionization and excitation of neutral hydrogen. Deep inside the molecular clouds, oxygen, nitrogen, carbon, and sulfur should then appear singly ionized. More highly ionized species should not be found, since charge exchange with neutral hydrogen would soon deplete doubly or more highly ionized species.

Optical radiation will only escape these dust clouds from an outer layer of roughly unit optical depth and will consist primarily of emission lines of H I, [O II], [S II], and [N II]. In contrast to the emission to be expected from star-forming regions, more highly ionized states would not be generally

observed. The observed relative strength of these low-ionization lines will depend on the ambient densities, since collisional de-excitation is important above the critical density, which differs appreciably for the different ionic transitions.

XI. LYMAN-ALPHA AND FREE-FREE EMISSION

We just saw that a low-temperature, ionized region forms at the leading edge of approaching clouds, even before they have actually collided with the sandwiched stationary layer. We now need to evaluate the amount of Ly α and free-free emission from this layer, from the hot plasma immediately behind the collision front, and from cooler plasma far downstream from the front (Fig. 4). We will consider these in turn.

a) Ahead of the collision front, the ionization front advances at a speed $F_i/n \approx 4 \times 10^8 \text{ cm s}^{-1}$, as long as the dominant absorption of radiation is due to ionization of atoms. For a cloud with grain number density n_g and typical grain extinction cross section σ_g , grain absorption dominates once photons have penetrated to a distance $(\sigma_g n_g)^{-1}$ into the approaching cloud. The cool precollision ionized layer, therefore, will have a depth d_g of order

$$d_g = 10^{19} \left(\frac{10^{-9} \text{ cm}^{-3}}{n_g} \right) \left(\frac{10^{-10} \text{ cm}^2}{\sigma_g} \right) \text{ cm}.$$

The rate of recombination along this line of sight is dictated by the recombination coefficient $\alpha(T)$:

$$\dot{N}_{\text{H}} = \alpha(T) n^2 d_g \approx \frac{2.5 \times 10^{-11}}{T^{1/2}} n^2 d_g \text{ cm}^{-2} \text{ s}^{-1} \\ \approx 2.5 \left(\frac{10^4 \text{ K}}{T} \right)^{1/2} \left(\frac{n}{10^3 \text{ cm}^{-3}} \right)^2 \left(\frac{d_g}{10^9 \text{ cm}} \right) \text{ cm}^{-2} \text{ s}^{-1} \ll F_i,$$

where we have set $n_i = n_e = n$, the ion and electron densities remaining essentially identical to the pre-ionization density of atoms.

Over the duration of infall, $d_g/v \approx 4 \times 10^{11} \text{ s}$, only a fraction $N_{\text{H}}/vn \approx 10^{-4}$ to 10^{-3} of the ions in this layer can recombine to provide Ly α emission. As we will see, this is a negligible fraction compared to the emission, in this spectral line, in the cooling region downstream of the collision.

The free-free emission from this layer in the Rayleigh-Jeans tail of the blackbody distribution will produce a surface brightness

$$I(\nu) = \frac{2\nu^2 kT}{c^2} K(\nu) d_g,$$

where $K(\nu)$ is the absorption coefficient at frequency ν :

$$K(\nu) = \frac{8}{3\sqrt{2\pi}} \frac{e^6}{c(mk)^{3/2}} \frac{n^2}{T^{3/2}} \ln \left(\frac{1.32k^{3/2}}{2\pi e^2 m^{1/2}} \frac{T^{3/2}}{\nu} \right) \text{ cm}^{-1} \\ = 10^{-2} \frac{n^2}{T^{3/2} \nu^2} \ln \left(5 \times 10^7 \frac{T^{3/2}}{\nu} \right) \text{ cm}^{-1},$$

so that for $K(\nu) d_g \ll 1$,

$$I(\nu) = 3 \times 10^{-39} \frac{n^2}{T^{1/2}} d_g \ln \left(5 \times 10^7 \frac{T^{3/2}}{\nu} \right) \\ \text{ergs cm}^{-2} \text{ s}^{-1} \text{ sr}^{-1} \text{ Hz}^{-1}.$$

The radio emission around 5 GHz is, therefore, virtually inde-

pendent of frequency, since $K(\nu)d_g \approx 0.04 \ll 1$. Hence,

$$I(\nu) \approx 3 \times 10^{-16} \left(\frac{10^4}{T} \right)^{1/2} \text{ ergs cm}^{-3} \text{ s}^{-1} \text{ sr}^{-1} \text{ Hz}^{-1}.$$

For a source like Arp 220, for which Condon (1980) found radio dimensions $1''.3 \times 0''.5$, the expected flux becomes

$$F_{\text{ff}}(\nu) \approx 2 \times 10^{-3} \text{ Jy},$$

which is two orders of magnitude less than the radio flux at these frequencies observed from Arp 220.

b) We next consider the hot, $T \approx 10^6$ K, layer just behind the shock. The relatively thin dimension $d \approx 8 \times 10^{15}$ cm and high temperature of this layer add up to a negligible recombination rate, opacity, and free-free emission rate despite the factor of 4 increase in density. This can be verified through use of the same expressions given above, by substituting the appropriate physical parameters for this layer.

c) Finally, we consider a layer downstream of the collision where partial recombination has already set in and where the temperature is $\sim 10^4$ K. This layer, whose thickness is $d\alpha$, separates the fully ionized gas just behind the collision from fully recombined gas even further downstream. It is kept largely ionized by far-ultraviolet photons emitted by the adjacent hot layers. In a steady state this layer balances ionization and recombination rates:

$$\mathcal{N}F_i = n_e n_i \frac{2.5 \times 10^{11}}{T^{1/2}} d \text{ cm}^{-2}.$$

Here $\mathcal{N} \geq 1$ is the number of ionizations directly and indirectly produced by each photon. Energy balance is given by

$$\left(\frac{nmv^3}{4} \right) \left(\frac{n_i}{n_a + n_i} \right)^{1/4} = (T)n_e n_i d,$$

where the expression between the first parentheses on the left is half the energy dissipated in the original collision—the other half being radiated outward into the approaching cloud—and the second expression in parentheses is the fraction of the energy going into heating the gas as distinguished from energy loss through ionization or excitation of atoms and ions. This expression is an estimate based on the work of Shull and Van Steenberg (1985), who have calculated these various energy deposition rates for energetic electrons, in our case the photoionization electrons. In this expression n_i and n_a , respectively, are the ionic and atomic density, and $n_i/(n_a + n_i)$ is the ionization fraction.

Combining the two equations for steady state equilibrium, we obtain

$$\begin{aligned} \mathcal{L}(T)T^{1/2} &\approx \left(\frac{nmv^3}{4} \right) \left(\frac{n_i}{n_a + n_i} \right)^{1/4} \frac{2.5 \times 10^{-11}}{\mathcal{N}F_i} \\ &\sim \frac{3.9 \times 10^{-22}}{\mathcal{N}} \left(\frac{n_i}{n_a + n_i} \right)^{1/4} \left(\frac{n}{10^3 \text{ cm}^{-3}} \right) \\ &\quad \times \left(\frac{v}{2.5 \times 10^7 \text{ cm s}^{-1}} \right)^3 \text{ ergs cm}^3 \text{ K}^{1/2} \text{ s}^{-1}. \end{aligned}$$

Now, $\mathcal{L}(T)T^{1/2}$ ranges from $\sim 10^{-21}$ at $T = 10^4$ to $\sim 3 \times 10^{-22}$ at $T \approx 10^3$ K. Hence $n_i/(n_a + n_i)^{1/4} \mathcal{N}^{-1}$ must have the maximum value it can assume, namely unity, in order for reasonable temperatures, consistent with a partially ionized gas, to obtain. This dictates the choice of $\mathcal{N} = 1$, $n_i/(n_a + n_i) \approx$

1, $T \approx 10^4$ K for this layer, and that temperature implies $\mathcal{L} = 10^{-23}$ ergs $\text{cm}^3 \text{ s}^{-1}$ (Fig. 5). We now are able to evaluate $d_d = 10^{13}$ cm and obtain the free-free emission rate from this layer, assuming that the electron and ion densities are prescribed by pressure equilibrium throughout the region.

$$\begin{aligned} F_{\text{ff}}(\nu) &= 5 \times 10^{-4} \left(\frac{n_e}{4 \times 10^5} \right)^2 \left(\frac{d_d}{10^{13} \text{ cm}} \right) \\ &\quad \times \left(\frac{10^4}{T} \right)^{1/2} \left(\frac{\Omega}{0''.65} \right) \text{ Jy}, \end{aligned}$$

which again is small compared to the flux from Arp 220.

Finally, we note, for self-consistency that total absorption in a layer can only be obtained with a thickness $d_d = (v/v_0)^3 \sigma(v_0)^{-1} n_a^{-1}$, where $\sigma(v_0)$ is the ionization cross section at the ionization edge v_0 . With $\sigma(v_0) \approx 10^{-17} \text{ cm}^2$ and $n_a \approx 4 \times 10^4$, we see that d_d will be of the order calculated. Here we have neglected magnetic field pressures, which will somewhat reduce the number densities in the cool downstream ionized region.

The Ly α radiation obtained can now be estimated. We note:

i) Each electron-ion pair recombines once in forming the neutral layer in the wake of the separating partially ionized downstream layer.

ii) Within the partially ionized layer, each photon of the F_i flux re-ionizes an already recombined atom, which then has to recombine a second time due to this effect.

iii) We notice that the ion formation rate ahead of the collision is far less than F_i per unit area. In the absence of dust the ionization front would proceed at a rate F_i/n , while with dust present, it will only proceed at a rate v . Hence the efficiency of ionization is only $nv/F_i \approx 0.0625$ for the photons penetrating the upstream region, and the overall number of recombinations, and thus the overall number of Ly α photons per extreme ultraviolet photon, is only $\frac{1}{2}$. Overall, we then have a Ly α flux corresponding to only half the flux of ionizing photons. However, since these photons will be an order of magnitude or two more energetic than those produced in H II regions, the ratio of Ly α flux to total radiated energy will also be correspondingly reduced. This would account for the very low Ly α flux inferred by Beck et al. (1986) and DePoy, Becklin, and Wynn-Williams (1986).

XII. PROPORTIONALITY OF THE RADIO AND INFRARED FLUXES IN STARBURST REGIONS AND COLLIDING GALAXIES

For starburst galaxies the infrared luminosity is attributed to radiation by luminous young stars which directly and indirectly heat dust grains in a surrounding cloud of gas and dust. The grains convert incident energy into FIR radiation, which then escapes the cloud. The radio emission is generally explained in terms of synchrotron emission from relativistic particles accelerated at the front of an expanding supernova shock wave. A starburst model explains the proportionality of radio and infrared fluxes by invoking the evolution of O and B stars to the supernova stage and demanding a constant proportionality between the young stars and the supernovae into which they are believed to evolve. If one starts with a larger aggregate of O and B stars, a proportionally larger issue of supernovae can be expected. In turn, these will provide a proportionally increased number of relativistic particles producing a radio flux which matches the rise in the luminosity of the stars and the grains they heat. In all of this, the ionized gases

surrounding the young stars are not portrayed as primary contributors to the radio flux or to X-ray emission; the X-ray emission from star-forming regions predominantly comes directly from the stellar coronae.

We now show that the fraction of the energy going into shock expansion and hence into cosmic-ray acceleration is about the same in colliding galaxies and in starburst regions. To the extent that relativistic particles also are the source of radio emission from galaxies, we therefore would expect a proportionality between far-infrared and radio emission to be a constant ratio for both these types of sources.

Reduced to quantitative terms, one can think of the energy going into infrared radiation to be a constant, large fraction of a star's luminosity integrated over its entire main-sequence existence. For an O star converting on the order of a solar mass of hydrogen into helium, that energy will amount to $\alpha M_{\odot} c^2$ with $\alpha \approx 10^{-2}$. The energy put into the expanding blast wave in a subsequent supernova explosion is of order $\beta M_{\odot} c^2$. In a typical supernova, in which roughly a solar mass is ejected at velocities of order 10^8 cm s $^{-1}$, $\beta \approx 10^{-5}$. The ratio of infrared-to-radio luminosity is then dependent on the ratio $\alpha/\beta \approx 1000$.

The question we need to answer is whether that ratio is unique to starburst regions or whether collision of molecular clouds can reproduce the same ratio.

By taking molecular clouds of thickness $Z = 2.7 \times 10^{20}$ cm and permitting them to collide at $v_a = 2v = 500$ km s $^{-1}$, the time for complete interpenetration was

$$t = \frac{3Z}{4v} \approx 8 \times 10^{12} \text{ s},$$

while the cooling time of the hottest, outermost plasma layers was

$$\tau = 1.24 \times 10^9 \text{ s}.$$

With two surfaces to the ionized layer, we see that $(2\tau/t) \approx 1/3000$ of the gas remains at a temperature of order 10^6 K, to expand back out into the still approaching halo gas at an initial relative velocity of order 500 km s $^{-1}$. This means that the ratio of energies available to produce infrared, as compared to radio emission, is $t/2\tau \approx 3000$. At somewhat lower densities than taken above, say $n \approx 300$, τ increases by a factor of 3, and $t/2\tau$ becomes 1000. Thus, since $t/2\tau$ is comparable to α/β , we see that within a factor of order unity the ratio of energies available for producing respectively infrared and radio luminosities will be the same in starbursts and in molecular cloud collisions.

It is worth noting that rapidly approaching central molecular disks of galaxies normally will be interacting with sandwiched halo gas, even before the molecular clouds come into contact. Appreciable cosmic-ray acceleration thus could even slightly precede actual cloud impact. The accelerated high-energy particles ultimately could penetrate through the approaching molecular clouds (Morfill, Meyer, and Lüst 1985) and escape the sandwiched layer, to enter the general interstellar medium.

XIII. COLLISIONS AMONG LOWER DENSITY CLOUDS

From time to time during the collision of two galaxies, low-density clouds will collide with each other or with higher density molecular clouds. Here, the initial density in the lower

density cloud will be of order $n \approx 1$ cm $^{-3}$, and a nearly adiabatic impact can increase its density to $n_e = n_p \approx 4$ cm $^{-3}$. The temperature again is determined by the initial kinetic energy of the approaching clouds and will be on the order of 10^6 K. In the case of a low-density cloud colliding with a cloud of appreciably higher density, relatively little translational velocity is imparted to the denser cloud, and the temperature in the low-density domain just behind the shock will be somewhat higher.

The cooling rate for a cloud whose initial density is $n = 1$ cm $^{-3}$ will be a factor of 10^3 below that of a cloud whose initial density is $n = 10^3$ cm $^{-3}$. The time constant for cooling, therefore, is of order 10^{12} s, while the interpenetration time of the smaller H I clouds will be $t \ll 8 \times 10^{12}$ s—far less than for molecular disks. Smaller tenuous clouds will therefore act almost elastically, in that they will re-expand after the collision without having given up an appreciable amount of energy through radiation. Moreover, the absence of appreciable amounts of dust in the low-density clouds implies that the relatively few photons radiated would lie in the extreme ultraviolet and therefore be difficult to detect—since interstellar gases in our own Galaxy, if not in the parent galaxy, will effectively absorb this radiation.

These elastically colliding clouds bounce back, expand, and interact with energetic particles, accelerating them to higher energies. That could considerably enhance the cosmic-ray energy density and hence the radio emission of the galaxies if the mass of low-density gas actively colliding were 10^{-3} or more times the mass of colliding molecular disks.

However, since the lifetime of cosmic rays before escape from a galaxy is only of order 10^{14} s, all these H I clouds would have to be colliding within 10^{14} s of the time the central molecular disks impact. The distance traveled during that time is ~ 2 kpc, at 5×10^7 cm s $^{-1}$. For 5° or smaller tilt angles between the planes of the colliding galaxies, radio emission therefore could coincide with the epoch of extreme FIR luminosity. In short, the general interstellar medium could appreciably contribute to the observed radio emission from ELFS. Not only the gases associated with the central disks will be involved, though those could most readily account for the direct proportion between infrared and radio luminosities.

XIV. MOLECULAR HYDROGEN EMISSION

In § IX we showed that a partially ionized layer at temperature $T < 6 \times 10^4$ K ≈ 5 eV can precede the collision front into the neutral clouds. Ultimately, the ionization fraction drops because of dust absorption. Beyond dust optical depths $\tau_{\text{dust}} \approx 1$, partially ionized gas will be found with a column density $N \approx \sigma_p^{-1}$ and depth $D \approx n^{-1} \sigma_p^{-1} \approx 10^{14}$ cm. We can expect that this partially ionized gas will have a fraction f_m of hydrogen molecules among its neutral constituents. The Einstein coefficient A for vibration-rotational transitions of excited molecules in the ground electronic state is of order $A = 10^{-6}$ s $^{-1}$, and since the survival time of the partially ionized layer is only $t_p \approx D/v \approx 4 \times 10^6$ s, typically each excited molecule can only radiate once before dissociation and ionization. Since the collision cross sections for hydrogen molecules colliding with other molecules or with atoms is of order $\sigma_c = 3 \times 10^{-16}$ cm 2 , and the proton velocity at the temperatures cited is $v_H < 3 \times 10^6$ cm s $^{-1}$, the time between excitations of a hydrogen molecule is $(nv_H \sigma_c)^{-1} = t_c > 10^6$ s.

We, therefore, expect only a few vibrational transitions per molecule in this layer. If $f_m \approx 0.3$ and each photon has an

energy of $\epsilon_{\text{H}_2} \approx 10^{-12}$ ergs, we would expect a flux of

$$F_{\text{H}_2} \approx \frac{Nf_2}{(t_c + A^{-1})} \epsilon_{\text{H}_2} \\ \approx 1.5 \times 10^{-2} \left(\frac{10^{-17}}{\sigma_p} \right) \left(\frac{f_2}{0.3} \right) \left(\frac{2 \times 10^6 \text{ s}}{t_c + A^{-1}} \right) \\ \times \left(\frac{\epsilon_{\text{H}_2}}{10^{-12} \text{ ergs}} \right) \text{ ergs cm}^{-2} \text{ s}^{-1},$$

integrated over all energy levels. This amounts to roughly 10^{-3} of the total radiative flux, $F \approx 12.5 \text{ ergs cm}^{-2} \text{ s}^{-1}$.

Since the collision time between molecules is on the order of the radiative lifetime, one may expect that some of the vibrational energy will be redistributed among colliding molecules and that this energy sharing will lead to a larger fraction of the energy radiated from low vibrational energy states. In the portion of the neutral cloud heated by the more highly penetrating hard photons, the temperature will rise slowly, and there too the lowest vibrational energy levels, principally the level $v = 1$, should be observed to radiate.

Joseph, Wright, and Wade (1984) note that the flux in the $v = 1-0$, $S(1)$ molecular hydrogen line for NGC 6240 and Arp 220, respectively, amounts to 10^{-4} and 10^{-5} of the total bolometric luminosity. They failed to detect the $v = 2-1$, $S(1)$ line for which they searched in NGC 6240 and would probably have detected it had its intensity been about half that of the corresponding $v = 1-0$ transition. DePoy, Becklin, and Wynn-Williams (1986) observe comparable, though somewhat lower, flux levels in NGC 6240 in the $v = 1-0$, $Q(1)$ and $v = 1-0$, $Q(3)$ lines and a combined H_2 flux level in the observed lines of $\sim 4 \times 10^{-4}$ of the bolometric flux observed.

Given all the uncertainties of our model, the rough calculation of expected molecular hydrogen line intensities appears to be in as reasonable agreement with observations as can be expected.

XV. CO EMISSION

Ultraviolet radiation emanating from the ionized region can be partly absorbed by hydrogen atoms or molecules or directly absorbed by grains. Grains will also tend to indirectly absorb energy originally invested in exciting atoms and molecules, since the optical and ultraviolet photons re-emitted by these particles again can be absorbed by grains. Some of the radiation given off in atomic recombination also suffers that fate. All in all, the radiation entering the cloud is efficiently converted into FIR radiation, since grains rapidly re-emit any absorbed light at these long wavelengths.

Molecular and atomic hydrogen cannot contribute to the cooling of gas at the low temperatures prevalent in normal molecular clouds. Only at the high temperatures that characterize molecular shocks can any direct cooling by hydrogen be anticipated. The gas in the cloud is therefore cooled primarily by impurity constituents, and a fair fraction of that cooling, at low temperatures, will be due to CO emission.

We now need to investigate the relationship between CO emission at 2.6 mm wavelength, where observations have been made, and the FIR luminosity of colliding galaxies: The FIR luminosity of such galaxies is dictated by two parameters, the mass of colliding material and the velocity of the collision.

At constant velocity, we would expect the infrared luminosity of colliding clouds to be directly proportional to the mass of gas interpenetrating at any instant. The molecular clouds

have been modeled, above, as having constant thickness. The mass of interacting gas would then simply be proportional to the area of the interacting clouds, and the CO emission should similarly be proportional to that area. That result is independent of the self-absorption of 2.6 mm radiation within the cloud. Under constant velocity conditions, then, we would expect that $L_{\text{CO}} \propto L_{\text{IR}}$.

The luminosity of interacting galaxies can, however, also be increased by increased velocity. The power supplied to the colliding layers is increased as v^3 , so that a doubling of the approach velocity can result in an eightfold increase in luminosity, other factors being kept constant. The infrared luminosity will then depend on v^3 as well, but the CO luminosity L_{CO} will rise far more slowly.

If gas is heated primarily by collisions with grains, its temperature will rise at a rate proportional to the difference between grain and gas temperatures, $T_{\text{gr}} - T_{\text{gas}}$. The grain temperature, however, only rises as $L_{\text{IR}}^{1/5}$. Hence, if the cooling rate through CO emission were proportional to the heating rate of the gas, we would have $L_{\text{CO}} \propto L_{\text{IR}}^{1/5}$, in this case.

We see, therefore, that we might expect the CO luminosity to rise at a rate somewhere between $L_{\text{IR}}^{1/5}$ and L_{IR} , for cloud-cloud collisions in colliding galaxies. It is therefore not too difficult to believe that in a set of galaxies in which both the mass of gas and the velocity of approach can vary, the proportionality $L_{\text{CO}} \propto L_{\text{IR}}^{2/3}$ would be observed, though with considerable scatter of the data. This is essentially what Sanders and Mirabel (1985) have reported.

It is still worth noting that some energy may also be supplied to the molecular gas by energetic electrons which escape the ionized cloud. Their energy also goes into ionization, excitation, and grain heating, as discussed in § X, and we would not expect the effect to change the relationship between the observed CO and FIR luminosities in any drastic way.

XVI. X-RAY EMISSION

While X-ray emission is not a universal feature of ELFS, an explanation for its occasional presence would be useful.

Although the ionized gases produced in the collision of molecular clouds in the rapidly approaching galaxies can have temperatures on the order of 10^6 K, no substantial X-ray emission can be expected unless these temperatures were to rise by a factor of 10, a prospect which is quite improbable. X-rays could, however, be produced in inverse Compton scattering of relativistic electrons interacting with infrared radiation. In this process photons with energies of order 10^{-2} eV are converted into photons with energies of order 10^3 or 10^4 eV, an energy increase of 10^5 – 10^6 requiring electrons with energy ϵ roughly in the range

$$10^{5/2} < \epsilon < 10^3 m_e c^2.$$

If these energetic particles are produced in the same region as the high infrared flux, the inverse Compton effect will be more probable.

As pointed out above, the acceleration of relativistic particles can take place even before cloud-cloud impact and also will take place after the molecular clouds have been consumed. At that later stage the infrared flux will be lowered. However, if one cloud is rather thicker than the other, parts of it will still persist after the thinner cloud has totally penetrated the ionized layer. One may then have the situation in which a high FIR flux emanates from a molecular cloud still penetrating one side of the ionized layer, while an expanding shock produces

relativistic particles at the opposite face of the layer. Because of their close proximity, the relativistic particles can then readily interact with the FIR radiation, to produce the X-ray flux. Most generally, however, relativistic particles produced early in cloud collisions will rapidly diffuse across the volume occupied by the interacting galaxies, and inverse Compton back-scatter FIR radiation wherever it is produced. The highest X-ray flux levels would be observed for thin layers meeting face on, at high velocities, and where the observer's line of sight is along the collision path. That way the X-rays need only penetrate a thin molecular layer. We would, therefore, expect the highest X-ray emission where CO lines are particularly wide and the FIR luminosity is high.

At the photon energies of interest, the collisional cross section for relativistic electrons with energies of order 1 GeV is the Thomson cross section $\sim 10^{-24}$ cm². With the X-ray photons $\sim 10^5$ times as energetic as the infrared photons, and the X-ray flux 10^{-3} times lower than the FIR flux, the probability for scattering an infrared photon needs only be 10^{-8} . In turn, that implies a relativistic electron column density $n_r \approx 10^{16}$ cm⁻². The mean cosmic-ray electron energy density per unit area of colliding clouds becomes $\sim 2 \times 10^{13}$ ergs cm⁻² for this column density, while the total kinetic energy per unit area for the colliding clouds is $nmv^2/2 \approx 2 \times 10^{16}$ ergs cm⁻². Only one part in 10^3 of the cloud energy would therefore need to be invested in the production of relativistic electrons.

The observed integrated radio flux similarly appears to be only one part in 10^3 of the integrated infrared flux (Sanders and Mirabel 1985). This implies that the magnetic field energy density encountered by the relativistic electrons emitting synchrotron radiation would need to be comparable to the infrared energy density through which the electrons stream. Since the infrared surface brightness of the clouds is of order $nmv^3/2$, the infrared energy density should be $\sim 3nmv^3/2c$, and the magnetic field energy density would be

$$\frac{B^2}{8\pi} \approx \frac{3nmv^3}{2c} \approx 10^{-9} \text{ ergs cm}^{-3},$$

$$B \approx 1.6 \times 10^{-4} \text{ gauss}.$$

This magnetic field strength is quite reasonable in a shocked region, and the fields could become quite extended without straining the available energy budget.

From an energetic viewpoint, at least, X-ray and radio wave production at the observed luminosities is quite consistent with the model we have sketched. A more detailed analysis would be required to investigate these emissions in greater depth. The picture still is quite speculative but would at least explain the occasional high X-ray flux observed in ELFS.

VII. PREDICTIONS

1. Far-infrared emission from the ionized layer between the sandwiching molecular clouds penetrates through the surrounding dust layers to reach our telescopes. We would expect to observe emission from [O IV] at 25.87 μ m and [Ne V] at 24.28 μ m—spectral lines previously detected in high-excitation planetary nebulae by Shure *et al.* (1983) and in NGC 1068 (Houck 1986). [Mg IV] 4.49 μ m and [Mg V] 5.6 μ m lines might also be sought. For observations possible with ground-based observatories, the [S IV] 10.4 μ m and [Na IV] 9.039 μ m lines might recommend themselves, though the sodium line has not been astronomically detected to date. At the 10^3 – 10^6 K temperatures calculated for the ionized layers, these and other

transitions of highly ionized elements should prevail in place of the [O III] 51.8 and 88.35 μ m lines or the transitions of N⁺⁺, S⁺, or S⁺⁺, more characteristic of H II regions at 10^4 K. Although these observational distinctions between starburst and colliding galaxies may not be possible today, the advent of the Infrared Space Observatory and SIRTf should provide the tools required to make this distinction.

2. In our model, X-ray emission through inverse Compton scattering is directed back toward the source of infrared radiation. The X-rays only reach us after passing through a molecular cloud and should have power-law spectra, exhibiting absorption—flattening or turnover—at low frequencies. For NGC 2992 and 5506, X-ray spectra have been recorded that show these traits (Reichert *et al.* 1985; Maccacaro, Perola, and Elvis 1982.) The strongest X-ray emission would be seen when the central disks of the galaxies are colliding face on, the system is viewed along the direction of collision, and collision velocities are high—implying large atomic or molecular bandwidths as a prerequisite for X-ray fluxes to be high.

3. Much in the same fashion as X-rays, we also would expect gamma-rays to be emitted by these sources. The ratio of gamma-ray-to-X-ray flux would be the same as the escaping ultraviolet-to-infrared flux. The ultraviolet radiation can only escape from the surface layers of molecular clouds that have completely interpenetrated or from colliding low-density clouds. The gamma photons would be expected at energies $\sim 10^4$ times higher than the X-ray photon energies, just as the extreme ultraviolet photons are 10^4 times as energetic as FIR photons. The gamma-ray energy flux expected should be of order $2\tau/t \approx 1/3000$ times lower than the X-ray energy flux received—the contribution of ultraviolet photons escaping during the final stages of collision.

VIII. DISCUSSION

Our model is able to explain the low line strength of moderately ionized species in ELFS, in a way that differs from the traditional starburst explanation (cf. Elston, Cornell, and Lebofsky 1985). There, the suggestion is that stars with high metallicity are present and that these emit predominantly low-energy photons unable to doubly ionize oxygen or other elements. That explanation, though plausible enough, does require a description of ELFS both in terms of the frequently observed proximity to an apparently interacting companion galaxy and in terms of the high metallicity of the starburst region. In contrast, the explanation we have offered requires only the actually observed interaction of galaxies; no requirements are placed on metallicity.

The low Ly α luminosities noted by DePoy, Becklin, and Wynn-Williams (1986) can also be explained. Ly α is a feature produced on recombination. In typical starburst galaxies, where stellar radiation might produce photons with average energies of order 15 eV, an appreciable fraction of the radiation reaching absorbing dust clouds is produced in recombination that leads to Ly α photon production. In ELFS the plasma at 10^6 K or greater emits photons with energies of order 100 eV. The Ly α energy amounts to only a small fraction of this. Hence about an order of magnitude more energy goes into FIR radiation per Ly α photon in our model for ELFS than in starburst galaxies.

Our model, whose main traits are summarized in Table 1, is also able to satisfactorily account for the other observed features we have listed. Clear-cut evidence for the collisional model can come from FIR fine-structure observations, which

TABLE 1
EMITTING REGIONS AT DIFFERENT STAGES OF ELFS EVOLUTION

Wavelength	Mechanism	Location	Time Scale for Face-On Impact (s)	Luminosity for Face-On Impact (L_{\odot})
Radio	Free-free Synchrotron	Ionized layers Surrounding the colliding disks	$\sim 10^{13}$ $\sim 10^{13}$	$\sim 10^8$ $10^9?$
CO FIR	Grain heating of CO UV-heated dust ~ 60 K	Surface layers of disks In pre-collision front ionized gases	$\sim 10^{13}$ $\sim 10^{13}$	10^{12}
H ₂ lines	Collisionally excited	Upstream of pre-collision ionization front, in partially ionized molecular cloud	$\sim 10^{13}$	$\sim 10^9$
Optical	Collisional excitation of singly ionized species, O ⁺ , S ⁺ , N ⁺ , ...		$\sim 10^{13}$	Partly absorbed in dust layers?
UV	Ionic line radiation in hot plasma	Rapidly expanding dust-collision layer	$\sim 3 \times 10^9$	Absorbed by interstellar gases
X-rays	Inverse Compton scatter of FIR photons	Surrounding colliding disk	$\sim 10^{13}$	$10^9??$
γ -rays	Inverse Compton scatter of UV photons	Rapidly expanding totally ionized region	$\sim 10^9$	$L_{X\text{-rays}}/3000$

should indicate the presence of highly ionized species normally found only in high-excitation planetary nebulae and not in star-forming regions. Fine-structure line ratios could also indicate the density of these high-temperature regions, which ought to be roughly 4 times higher than densities in the colliding molecular clouds.

Among a random distribution of galaxies, one could expect that only one such pair among roughly 10^5 galaxies would be found with an internuclear distance of 30 kpc. In contrast, the fraction of galaxies generally classed as interacting is more like 1%. That tells us that interacting galaxies cannot simply be galaxies in chance encounter. Many may have had an initial interaction at earlier times when the universe was more compact and might have been captured into a distant orbit at that time. Such pairs will have effective interactions on time scales of order 10^8 yr, and the orbits they describe will change appreciably as time goes on, particularly if there are other nearby galaxies, perhaps other members of a small group to which the pair belongs.

If this were not so, the chances that a random perturbation would bring two galaxies within 1–2 kpc of each other would be remote. But with galaxies in close proximity interacting from time to time, the chances of a close encounter become appreciable. This is important to note, since the credibility of the model hinges on just this point. In that sense it is worth

noting that recent observations by Sargent (1986) show CO emission concentrated within spans of 1.5 kpc for Arp 220 and NGC 3690 and 2.5 kpc or less for NGC 7469 and NGC 6240. Unless there is reason to believe that most of these objects are not interacting galaxies, one has to take seriously the idea that galaxies do interact, that some of these are extremely gas-rich, and that the consequences of a close collision will be the generation of a great deal of infrared emission.

A question worth pursuing further is the relationship of ELFS to some galaxies classified as Seyferts. Like Seyfert galaxies, ELFS will have broad emission over the central portion of galaxies in very close collision. FIR fine-structure radiation due to highly ionized species, like those observed in NGC 1068, if found in many Seyferts, could make a collisional model attractive for explaining the presence of these high-temperature gases.

We thank Drs. Chernoff, C. Cesarsky, and M. Cassé for incisive comments. G. G. C. P. acknowledges Drs. E. A. Boldt and S. S. Holt for their generous hospitality during his stay at NASA/GSFC as a NRC/NAS Research Associate. At Cornell, this work was supported by NASA grant NAGW-761 and JPL contracts 954603 and 957701. B. T. S. is supported by NASA under the *IRAS* Extended Mission Program.

REFERENCES

- Aaronson, M., and Olszewski, E. W. 1984, *Nature*, **309**, 414.
 Allen, D. A., Roche, P. F., and Norris, R. P. 1985, *M.N.R.A.S.*, **213**, 67P.
 Beck, S. C., Turner, J. L., and Ho, P. T. P. 1986, *Ap. J.*, **309**, 70.
 Condon, J. J. 1980, *Ap. J.*, **242**, 894.
 DePoy, D. L., Becklin, E. E., and Wynn-Williams, C. G. 1986, *Ap. J.*, **307**, 116.
 Draine, B. T., and Salpeter, E. E. 1979, *Ap. J.*, **231**, 77.
 Elston, R., Cornell, M. E., and Lebofsky, M. J. 1985, *Ap. J.*, **296**, 106.
 Fabbiano, G., Feigelson, E., and Zamorani, G. 1982, *Ap. J.*, **256**, 397.
 Fabbiano, G., and Trinchieri, G. 1985, *Ap. J.*, **296**, 430.
 French, H. B. 1980, *Ap. J.*, **240**, 41.
 Gaetz, T. J., and Salpeter, E. E. 1983, *Ap. J. Suppl.*, **52**, 155.
 Harwit, M. 1973, *Astrophysical Concepts* (Ithaca, N.Y.: Concepts).
 Harwit, M. O., and Pacini, F. 1975, *Ap. J. (Letters)*, **200**, L127.
 Helou, S., Soifer, B. T., and Rowan-Robinson, M. 1985, *Ap. J. (Letters)*, **298**, L7.
 Hollenbach, D., and McKee, C. F. 1979, *Ap. J. Suppl.*, **41**, 555.
 Houck, J. R. 1986, unpublished.
 Houck, J. R., Schneider, D. P., Danielson, G. E., Beichman, C. A., Lonsdale, C. J., Neugebauer, G., and Soifer, B. T. 1985, *Ap. J.*, **290**, L5.
 Joseph, R. D., Meikle, W. P. S., Robertson, N. A., and Wright, G. S. 1984, *M.N.R.A.S.*, **209**, 111.
 Joseph, R. D., Wright, G. S., and Wade, R. 1984, *Nature*, **311**, 132.
 Lawrence, A., Walker, D., Rowan-Robinson, M., Leech, K. J., and Penston, M. V. 1986, *M.N.R.A.S.*, **219**, 687.
 Lequeux, J. 1985, in *Naissance et enfance des étoiles, Birth and Infancy of Stars*, ed. R. Lucas, A. Omont, and R. Stora (Les Houches, Session 41) (Amsterdam: North-Holland), p. 3.
 Miller, G. E., and Scalo, J. M. 1979, *Ap. J. Suppl.*, **41**, 513.
 Morfill, G. E., Meyer, P., and Lüst, R. 1985, *Ap. J.*, **296**, 670.
 Palumbo, G. G. C., Fabbiano, G., Fransson, C., and Trinchieri, G. 1985, *Ap. J.*, **298**, 259.
 Reichert, G. A., Mushotzky, R. F., Petre, R., and Holt, S. S. 1985, *Ap. J.*, **296**, 69.
 Rieke, G. H., and Low, F. J. 1972, *Ap. J. (Letters)*, **176**, L95.

- Rubin, V. C., Burstein, D., Ford, W. J., Jr., and Thonnard, N. 1985, *Ap. J.*, **289**, 81.
- Sanders, D. B., and Mirabel, I. F. 1985, *Ap. J. (Letters)*, **298**, L31.
- Sanders, D. B., Solomon, P. M., and Scoville, N. Z. 1984, *Ap. J.*, **276**, 182.
- Sargent, A. 1986, paper presented at Symposium on Star Formation in Galaxies, Pasadena.
- Schweizer, F. 1986, *Science*, **231**, 227.
- Shull, J. M., and Van Steenberg, M. E. 1985, *Ap. J.*, **298**, 268.
- Shure, M. A., Herter, T., Houck, J. R., Briotta, Jr., D. A., Forrest, W. J., Gull, G. E., and McCarthy, J. R. 1983, *Ap. J.*, **270**, 645.
- Soifer, B. T., *et al.* 1984a, *Ap. J. (Letters)*, **283**, L1.
- Soifer, B. T., *et al.* 1984b, *Ap. J. (Letters)*, **278**, L71.
- Soifer, B. T., Sanders, D. B., Neugebauer, G., Danielson, G. E., Lonsdale, C. J., Madore, B. F., and Persson, S. E. 1986, *Ap. J. (Letters)*, **303**, L41.
- Telesco, C., and Harper, D. A. 1980, *Ap. J.*, **235**, 392.
- Trinchieri, G., Fabbiano, G., and Palumbo, G. G. C. 1985, *Ap. J.*, **290**, 96.
- Watson, M. G., Stanger, V., and Griffiths, R. E. 1984, *Ap. J.*, **286**, 144.
- Wright, G. S., Joseph, R. D., and Meikle, W. P. S. 1984, *Nature*, **309**, 430.

M. HARWIT and J. R. HOUCK: Department of Astronomy, Space Sciences Building, Cornell University, Ithaca, NY 14853-0355

G. G. C. PALUMBO: NASA/Goddard Space Flight Center, Greenbelt, MD 20771

B. T. SOIFER: Division of Physics, Mathematics, and Astronomy, Downes Laboratory, 320-47, California Institute of Technology, Pasadena, CA 91125